Journal of Geophysical Research: Oceans

RESEARCH ARTICLE
10.1029/2018JC014147

Atlantic Water Transformation Along Its Poleward Pathway Across the Nordic Seas

Anthony Bosse[1], Ilker Fer[1], Henrik Søiland[2], and Thomas Rossby[3]

[1]Geophysical Institute and Bjerknes Center for Climate Research, The University of Bergen, Bergen, Norway, [2]Institute of Marine Research and Bjerknes Center for Climate Research, Bergen, Norway, [3]Graduate School of Oceanography, University of Rhode Island, Kingston, RI, USA

Key Points:
- Large ocean heat loss triggers winter mixing of the Atlantic Water and spiciness injection
- The western Lofoten Basin is a hotspot for Atlantic water transformation
- Spiciness at the exit of the Nordic Seas responds within 1 to 1.5 years to the variability of Atlantic Water at Svinøy section

Correspondence to:
A. Bosse,
anthony.bosse@uib.no

Citation:
Bosse, A., Fer, I., Søiland, H., & Rossby, T. (2018). Atlantic water transformation along its poleward pathway across the Nordic Seas. *Journal of Geophysical Research: Oceans, 123*. https://doi.org/10.1029/2018JC014147

Received 4 MAY 2018
Accepted 11 AUG 2018
Accepted article online 23 AUG 2018

Abstract The warm and salty Atlantic Water is substantially modified along its poleward transit across the Nordic Seas, where it reaches deeper isopycnals. In particular, the Lofoten Basin, exposed to intense air-sea interactions, plays a crucial role in the transformation of Atlantic Water. Averaged over a seasonal cycle, Atlantic Water releases approximately 80 W/m^2 of heat to the atmosphere over a large area, leading to winter mixed layer depths of up to 500 m (locally exceeding 1,000 m in the Lofoten Basin Eddy, a permanent vortex located in the basin center) and substantial water mass transformation. We investigate spiciness injection (temperature and salinity increase) by winter mixing, by performing an isopycnal analysis using a comprehensive observational data set covering the 2000–2017 period. Compared to the Atlantic Water properties at the Svinøy section, representative of the inflowing Atlantic Water, some isopycnals reveal an important warming (up to 1.5°C) and salinification (up to 0.2 g/kg). Key areas for spiciness injection are the western Lofoten Basin and west of Bear Island. The modified spicy Atlantic Waters coincide with low potential vorticity with strongly density-compensated layers at their base, allowing double-diffusion processes to occur farther downstream toward the Arctic. Despite its limited spatial extent, the Lofoten Basin Eddy exhibits the greatest spiciness injection, as well as the deepest mixed layer and thickest low potential vorticity layer of the Norwegian Seas. The Atlantic Water spiciness at Svinøy shows a downstream correlation in the Lofoten Basin and farther north toward the Arctic with a lag of 1 to 1.5 years.

Plain Language Summary The warm and salty Atlantic Water is an important component of the ocean conveyor belt transporting heat from the equator to the pole. Substantial transformations of this water mass occur along its poleward transit across the Nordic Seas. The transformed waters, in response to winter cooling from the atmosphere, become denser and can be tracked by following the properties of seawater along surfaces of same density. The Lofoten Basin is a region, where warm and salty Atlantic Water accumulates within a 500-m-thick layer. Intense atmospheric cooling in winter is able to mix Atlantic Water all the way down to 500 m, thus playing a crucial role in its transformation. The area west of Bear Island also plays an important role in this process. The transformed Atlantic Water has a vertical structure allowing for slow diffusive processes to occur farther downstream in the Arctic. The Atlantic Water properties at the entrance of the Nordic Seas are correlated with the Lofoten Basin and farther north toward the Arctic with a lag of 1 to 1.5 years.

1. Introduction

The Nordic Seas are a key component of the global thermohaline circulation. The warm and saline Atlantic Water (AW) is modified under the action of intense cooling before it reaches the Arctic Ocean. The poleward circulation of AW has a major influence on the climate prevailing over western Europe (Årthun et al., 2017; Rhines et al., 2008). Surface cooling occurs in winter as a result of strong temperature gradient at the air-sea interface. In the eastern part of the Nordic Seas, this transforms AW into intermediate yet still warm and salty waters (Eldevik et al., 2009; Isachsen et al., 2007; Segtnan et al., 2011). At the northern edge of the Nordic Seas, AW strongly impacts the sea ice extent around Svalbard (Ivanov et al., 2016; Meyer et al., 2017; Onarheim et al., 2014; Peterson et al., 2017) and in the Barents Sea (Årthun et al., 2012; Lind et al., 2018), with important consequences on primary production and fish habitats (Fossheim et al., 2015; Oziel et al., 2017), as well as on weather and climate (Vihma, 2014). Understanding the processes controlling the transformation and variability of the AW properties is thus of crucial importance.

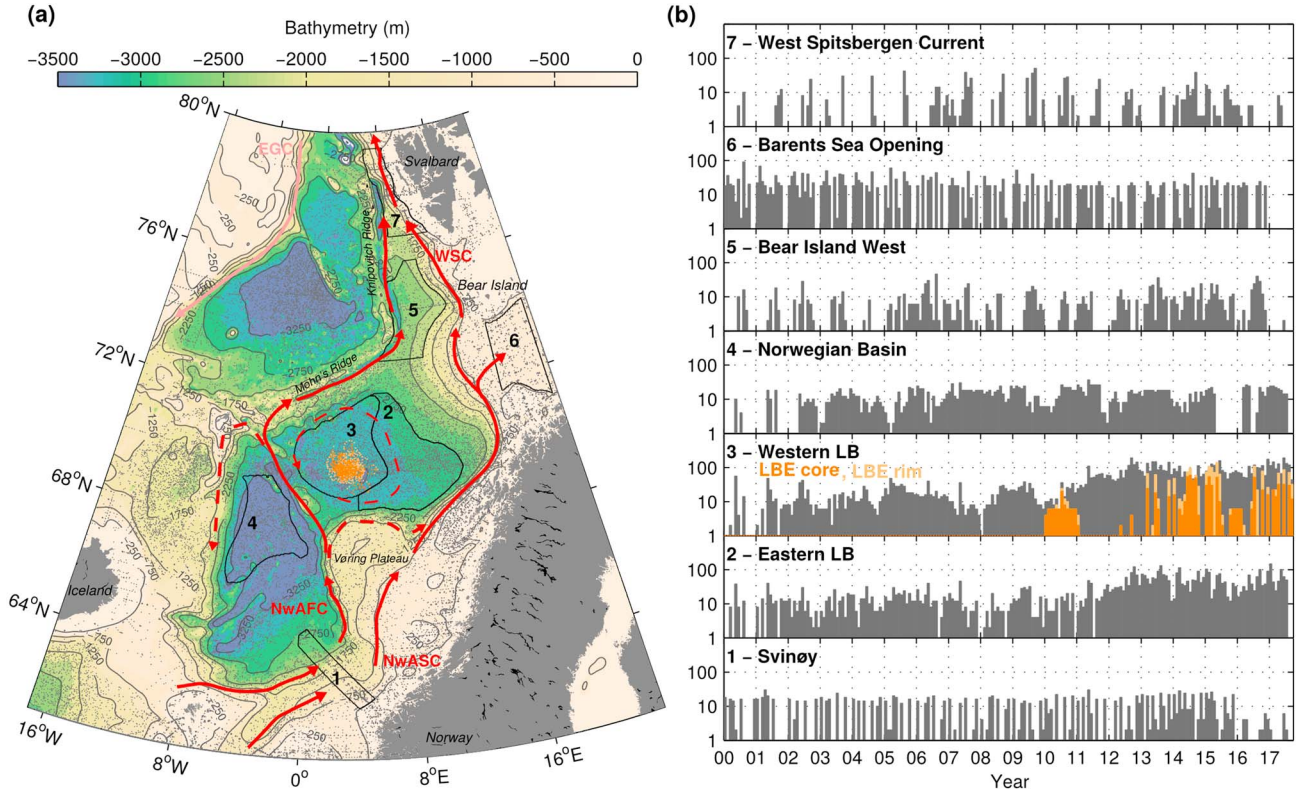

Figure 1. (a) Map of the state-binned profiles (see text) obtained by merging of various sampling platforms (shipborne CTDs, Argo floats, gliders). The main circulation patterns of the AW are shown by red arrows. Bathymetry is color shaded and contoured every 500 m starting from 250 m. Regions of interest are enclosed and marked 1 to 7. Dark and light orange dots are profiles in the LBE core and at the LBE rim, respectively. (b) Histograms of monthly observations from 2000 to 2017, in regions 1 to 7. AW = Atlantic Water; LBE = Lofoten Basin Eddy; EGC = East Greenland Current; WSC = West Spitsbergen Current; NwAFC = Norwegian Atlantic Frontal Current NwASC = Norwegian Atlantic Slope Current; LBE = Lofoten Basin Eddy; LB = Lofoten Basin.

Two major branches of AW connect the North Atlantic to the Nordic Seas between Iceland and Shetland (Figure 1). The Norwegian Atlantic Slope Current (NwASC) follows the shelf break roughly along the 500-m isobath. This branch can interact with the Norwegian Coastal Current carrying fresh waters from the Baltic Sea and continental runoff, especially off the Lofoten Islands where the shelf is particularly narrow. The second branch, the Norwegian Atlantic Frontal Current (NwAFC), appears as a jet associated with the Polar Front (separating warm/salty AW from cold/fresh polar waters). It is the westernmost extension of the warm and saline AW (Mork & Blindheim, 2000; Orvik & Niiler, 2002). The NwAFC typically flows along the 2,000-m isobath in the southern Nordic Seas, veers west around the Vøring Plateau, and continues poleward along mid-ocean ridges: the Mohn's Ridge in the Lofoten Basin (LB) and the Knipovich Ridge farther north (Orvik & Niiler, 2002). Toward Fram Strait, the NwAFC joins the slope current, called the West Spitsbergen Current (WSC) at these latitudes. The volume transport of AW of the slope and frontal branches is approximately 3.5–4 Sv each at Svinøy section (63°N), with a large variability at seasonal to interannual timescales (Høydalsvik et al., 2013; Orvik et al., 2001). Altogether, the AW currents constitute a poleward heat transport of about 300 TW entering the Nordic Seas (Hansen & Østerhus, 2000). Note, however, that this estimate is not from a closed section with a net zero volume transport (Schauer & Beszczynska-Möller, 2009).

AW exits the Nordic Seas through two main paths connected to the Arctic Ocean. In Fram Strait, the slope branch of the WSC carries around 1.3 Sv of warm AW to the Arctic (Beszczynska-Möller et al., 2012), while most of the outer branch (continuation of the NwAFC) recirculates southward in the East Greenland Current (Bourke et al., 1988; Hattermann et al., 2016; Manley, 1995). At the Barents Sea Opening (BSO)—a 400-m deep trench allowing AW to flow into the Barents Sea—Skagseth et al. (2008) estimated about 50 TW of heat transport (again, this is a partial section estimate with nonzero net volume transport), most of which is lost to the atmosphere before reaching the Arctic. The reader is referred to Beszczynska-Möller et al. (2011) for a complete review on the connection between the Nordic Seas and the Arctic Ocean.

Along its poleward pathway, AW passes through the LB: a 3,200-m-deep topographic depression with 400-km diameter, bounded by the Vøring Plateau in the south, the Norwegian shelf in the east, and the Mohn's sRidge in the northwest (Figure 1a). It is located between the two poleward branches of AW. The drift of Argo floats at middepth showed a cyclonic circulation in the inner part of the LB (Voet et al., 2010; dashed line in Figure 1a). The LB plays a particularly important role for the poleward transformation of AW, as being the largest heat and salt reservoir of the Nordic Seas (Björk et al., 2001; Mork et al., 2014). The AW layer reaches a maximum thickness of about 800 m in the deepest part of the basin. Intense heat losses prevail in winter with monthly net heat fluxes of more than 200 W/m^2 resulting in an annual heat flux from the ocean to the atmosphere of about 80 W/m^2 (Isachsen, 2015; Richards & Straneo, 2015; Rossby, Prater, & Søiland, 2009). As a consequence, deep winter mixed layer depths (MLD) exceeding 500 m are observed in the LB (Latarius & Quadfasel, 2016; Nilsen, 2006). In addition to the strong vertical mixing, the LB is characterized by an intense mesoscale eddy activity (see, e.g., Koszalka et al., 2011; Poulain et al., 1996; Raj et al., 2016; Rossby, Prater, & Søiland, 2009; Volkov et al., 2013) and stands out as a region with maximum eddy kinetic energy in the Nordic Seas. Eddies play a crucial role in the lateral heat and salt transfer from the slope to basin interior (Isachsen et al., 2012), where heat can accumulate before being surrendered to the atmosphere.

A particular feature of the LB circulation is the so-called *Lofoten Basin Eddy* (LBE): an anticylonic eddy, first observed and described by the Russian oceanographic surveys (Alexeev et al., 1991; Ivanov & Korablev, 1995a, 1995b). Since then, evidence has grown that the LBE might be permanent (Søiland et al., 2016). During the last decade, regular observations using ships (Søiland & Rossby, 2013) and gliders (Yu et al., 2017) have captured its coherence from year to year and depicted its general characteristics: 1,000- to 1,200-m-thick core of AW swirling with peak velocities up to 0.8 m/s at depth of 600–800 m and radial distance of 15–20 km. The eddy stays in the deepest part of the basin close to 70°N–3°E (Søiland & Rossby, 2013; Yu et al., 2017). The bathymetric depression acts as an attractor for anticyclones shed from the slope current. Mergers with those eddies, as well as deep winter mixing, have been recognized as important processes contributing to the longevity of this unique energetic eddy (Ivanov & Korablev, 1995a; Köhl, 2007; Volkov et al., 2015).

Spiciness is a concept that characterizes density-compensated temperature and salinity gradients in seawater. On a same density level, seawater can either be warm and salty (i.e., spicy) or cold and fresh (Munk, 1981). For instance, AW is a warm and salty water mass compared to cold and fresh polar waters of same density. From a general perspective, spicy waters are formed in the subtropics by the strong evaporation and vertical mixing (Kolodziejczyk et al., 2015; Yeager & Large, 2004) before flowing poleward along with western boundary currents (Laurian et al., 2006). At higher latitudes, those waters play an important role in air-sea interactions and oceanic heat transport (Kwon et al., 2010). As the spicy waters cool down in their poleward transit, they are transformed and reach deeper isopycnals. The corresponding patterns of spiciness transformation can be informative about the general circulation, especially in the Nordic Seas, a major high-latitude reservoir of spicy waters exposed to intense air-sea interactions.

Surprisingly, little attention has been given to spiciness in high-latitude oceanic basins. An earlier study by Rossby, Ozhigin, Ivshin, and Bacon (2009) reported a poleward increase in spiciness in the Nordic Seas along particular isopycnals. We conduct here a similar isopycnal analysis to describe in more detail the spatial and temporal AW transformation using spiciness as a state variable. The large number of observations from 2000 to 2017 has enabled to describe AW from seasonal to interannual timescales in key regions of the Nordic Seas, including those connected to the Arctic. The recent use of autonomous platforms such as Argo floats and gliders greatly improved the number of observations, especially within the LBE and more generally during winter, when shipborne measurements are sparse.

In the following, we first describe the main properties of AW from observations, as well as winter vertical mixing in the Nordic Seas. Next, spiciness distribution is evaluated along isopycnals, and geographical hot spots for water mass transformation are described. Finally, temporal variability of spiciness is examined in relation to winter mixing and AW inflow variability and timescales of propagation are estimated.

2. Data and Methods

2.1. Hydrographical Data Set

A hydrographical data set of the Nordic Seas is constituted by gathering observations from different sources for the 2000–2017 period, between 61–80°N and 17°W–23°E. A total of 43,993 shipborne Conductivity, Temperatrure and Depth (CTD) profiles was downloaded from the ICES database. In addition, 1,246 were obtained

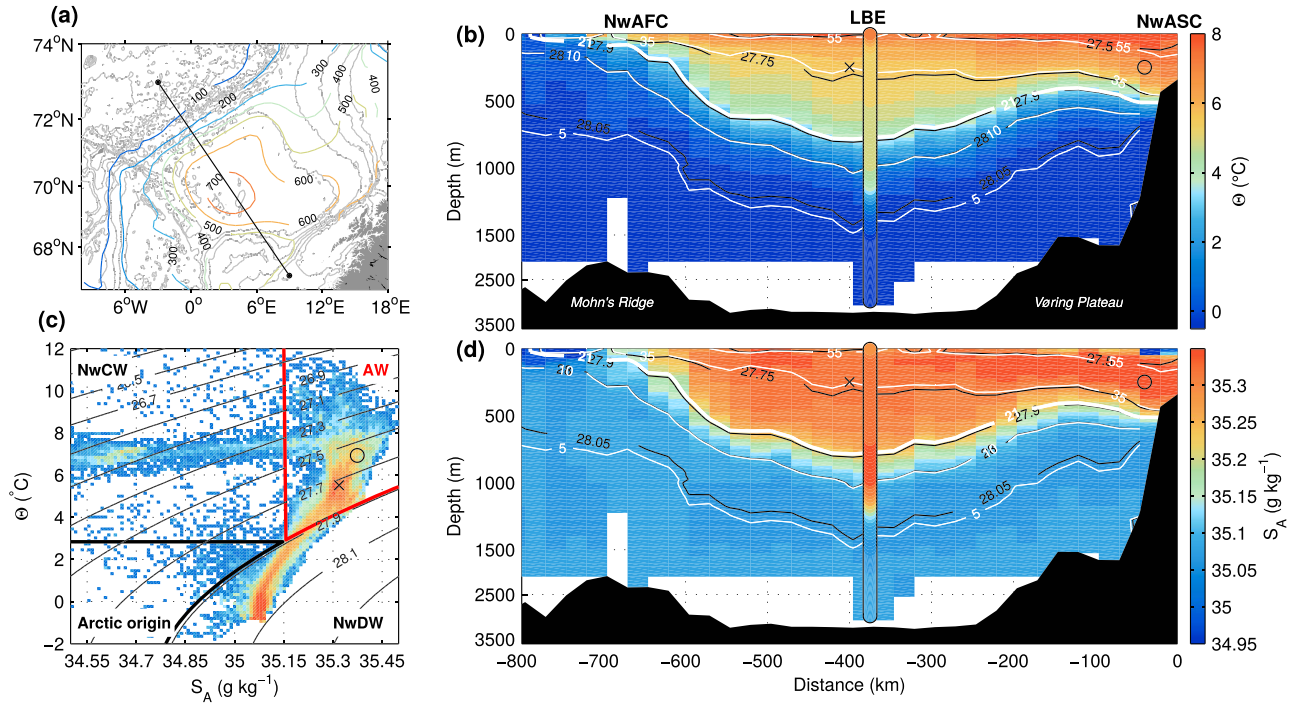

Figure 2. (a) Map of the Lofoten Basin with isobaths and colored contours showing the depth of δ_{21}. The black line indicates the cross-basin section shown in right panels. Vertical sections of (b) conservative temperature and (d) absolute salinity through the Lofoten Basin constructed by averaging profiles at less than 50 km from the section into 10 km by 10-m bins. Selected contours are shown for δ (white) and σ_0 (black). Note that the profiles in the LBE core and rim are excluded. A column separately shows the corresponding signal within the LBE. (c) Probabilistic Θ/S_A diagram from the profiles used to construct the cross-basin section. Main water masses are outlined. Colors refer to an arbitrary log scale of counts in Θ/S_A bins. The circle and the cross mark the two water parcels at the same depth, indicated in panels (b) and (d). NwAFC = Norwegian Atlantic Frontal Current; LBE = Lofoten Basin Eddy; NwASC = Norwegian Atlantic Slope Current; AW = Atlantic Water.

from the Institute of Marine Research via the Norwegian Marine Data center for the Svinøy, Gimsøy, BSO, and Bear Island sections, as well as dedicated cruises in the LB. A total of 22,117 profiles collected by autonomous Argo floats was retrieved from the Coriolis data center (Argo, 2000). Finally, 10 glider missions (12,461 profiles) carried out in the LB by the University of Bergen (NACO and PROVOLO projects) were finally added to the data set. Details on the data processing and scientific results from the glider missions can be found in Fer and Bosse (2017) and Yu et al. (2017). Prior to merging, the data from different sources were consistently interpolated on a 5-dbar pressure grid. Duplicates from various sources were identified as pairs of profiles collected less than 1 day and 1 km apart and removed.

A data set combining observing platforms with different temporal and spatial resolution must be homogenized. Following Gary et al. (2018), we perform *state binning* and isopycnally average data collected within one baroclinic deformation radius (15 km) and within 10 days. We choose shorter spatial and temporal scales than Gary et al. (2018; 25 km and 1 month), as mesoscale is characterized by smaller spatial and temporal scales in high-latitude environments. Out of a total of 77,625 initial profiles, the final data set product is composed of 57,753 state-binned profiles.

The geographical distribution of the merged data set exhibits a high density of observations in the LB (Figure 1a). The monthly data coverage in different regions of interest across the Nordic Seas is satisfactorily continuous (Figure 1b), especially in the LB, despite winter gaps in the northernmost regions (BSO, Bear Island West [BIW] and WSC). The Norwegian Basin (NB) has a good winter observational coverage thanks to Argo floats. The LB is by far the best sampled region by Argo floats, shipborne measurements (Gimsøy section and dedicated cruises), as well as gliders, which provide a very good data coverage in all seasons.

2.2. Detecting the LBE

The hydrography of the LBE is distinct from the general characteristics of the LB. Profiles in the LBE thus need to be set apart when describing the general basin properties. In order to do so, a simple criterion based on the Conservative Temperature averaged between 900 and 1,000 m was defined ($\Theta_{900-1000}$). While in the basin this depth range is below the warm AW (Figures 2b and 2d), within the LBE AW reaches 1,200 m. Yu et al. (2017)

observed a monotonic decrease in $\Theta_{900-1000}$ with the distance from the LBE center, r: from about 4.5 °C at the eddy center ($r < 20$ km) to about 0 °C away from its influence ($r > 40$ km). Based on this, we apply a simple criterion to the whole data set: *LBE core profiles* are those with $\Theta_{900-1000} > 4.5$ °C and *LBE rim profiles* those with 2.5 °C $< \Theta_{900-1000} < 4.5$°C. The LBE core and rim must be distinguished, because the $\Theta - S$ characteristics in the core are consistent from year to year, whereas the rim, typically 20 to 40 km from the eddy center, acts like a buffer and has more variable, yet still warm, properties (Yu et al., 2017). A rim profile is accepted only when it is accompanied by a core profile (within 15 days and 80 km), to ensure that it is not mistaken with other mesoscale eddies characterized by warm and deep AW (Richards & Straneo, 2015; Søiland et al., 2016). This criterion was tested against shipborne observations of the LBE from 2011 to 2017 (Fer et al., 2018; Søiland et al., 2016; Søiland & Rossby, 2013). It also performed well to identify the LBE from Argo floats. In particular, in 2010, a profiling float remained trapped in the LBE for approximately 1 year.

2.3. Diagnostics

Conservative temperature, Θ, absolute salinity S_A, specific volume anomaly, δ, and other oceanographic variables (e.g., vertical Turner angle, buoyancy frequency, and potential vorticity [PV] described below) were derived using the open-access Gibbs-Sea Water Oceanographic Toolbox (McDougall & Barker, 2011). As stated by Rossby, Ozhigin, Ivshin, and Bacon (2009), different ocean state variables can be used to describe *isopycnality*: with increasing accuracy, surfaces of constant potential density σ_0, specific volume anomaly referenced at the surface δ, and neutral surface γ^n (McDougall, 1989). For consistency with Rossby, Ozhigin, Ivshin, and Bacon (2009) and other studies, we here use δ as a proxy for the neutral surface.

AW is defined from a double criteria on specific volume anomaly ($\delta > 21 \times 10^{-8}$ m^3/kg, equivalent to $\sigma_0 \sim 27.9$ kg/m^3) and absolute salinity ($S_A > 35.15$ g/kg). The criterion on δ is the same used in previous studies (e.g., Mork et al., 2014; Rossby, Ozhigin, Ivshin, & Bacon, 2009). The δ_{21} surface successfully separates AW from the Norwegian Sea Intermediate Water, characterized by a salinity minimum between 1,000 and 1,500 m in the LB (Blindheim, 1990; Figure 2d). In addition, the salinity criterion distinguishes AW from fresh water of coastal or polar origin (Figure 2c). In the following analysis, AW thinner than 100 m are discarded.

The water column heat content is calculated from: $HC = \int \rho_0 c_p(\Theta - \Theta_{\text{ref}})$ with $\rho_0 = 1,028$ kg/m^3, c_p the specific heat of seawater and $\Theta_{\text{ref}} = -1$ °C, a reference temperature typical of deep waters in the Nordic Seas. The freshwater content is classically estimated using a reference $S_{\text{ref}} = 35$ g/kg (corresponding to a practical salinity of approximately 34.83): FWC $= \int (S_{\text{ref}} - S_A)/S_{\text{ref}}$.

The vertical Turner angle Tu is diagnosed from the temperature and salinity profiles smoothed by a 25-m moving average, $Tu = atan(\alpha\partial_z\Theta + \beta\partial_z S_A; \alpha\partial_z - \Theta\beta\partial_z S_A)$. Tu characterizes the stability of the water column with values between −90° and +90° (Ruddick, 1983). When a stabilizing vertical temperature gradient ($\partial_z\Theta > 0$) is associated with a destabilizing vertical salinity gradient ($\partial_z S_A < 0$), $Tu > 45°$. As Tu approaches 90°, temperature and salinity gradients tend to be perfectly density compensated (i.e., $\alpha\partial_z\Theta = \beta\partial_z S_A$ with α and β being the (positive) coefficients of thermal expansion and haline contraction).

PV is approximated as follows: $PV = fN^2/g$, where N^2 is the squared buoyancy frequency. This definition neglects the vorticity contribution of oceanic currents. It is here used as a proxy for winter vertical mixing and water mass transformation. MLD is defined using a density difference of 0.03 kg/m^3 relative to the average value of the upper 15 m (de Boyer Montégut et al., 2004). When specified, winter refers to the period from December to April and summer from June to October.

2.4. Definition of Spiciness

The density of seawater is determined by its temperature and salinity. Thus, temperature and salinity may vary along a surface of constant density. This variability, sometimes called *spiciness*, is a result of air-sea fluxes, turbulent mixing, and advection. The concept of a passive thermodynamic variable *normal* to density surfaces on the T/S space has been a long-standing question (Mamayev, 1962; Munk, 1981; Stommel, 1962; Veronis, 1972).

Variations in seawater density at a given temperature, salinity, and reference pressure (p_r) can be linearized as follows: $\mathrm{d}\rho = \beta(S,T,p_r)\mathrm{d}S - \alpha(S,T,p_r)\mathrm{d}T$. The idea behind spiciness, π, is to construct a quantity whose differential obeys $\mathrm{d}\pi = \beta(S,T,p_r)\mathrm{d}S + \alpha(S,T,p_r)\mathrm{d}T$, orthogonal to density lines in the $(\alpha T, \beta S)$ space (Munk, 1981; Stommel, 1962). Because of nonlinearities of the equation of state of seawater, this differential equation is not a total derivative and cannot be solved explicitly. This led to alternative definitions. Jackett and McDougall (1985) constrained π to be proportional to the isopycnal contrast of water masses in density units ($\int 2\beta\mathrm{d}S$),

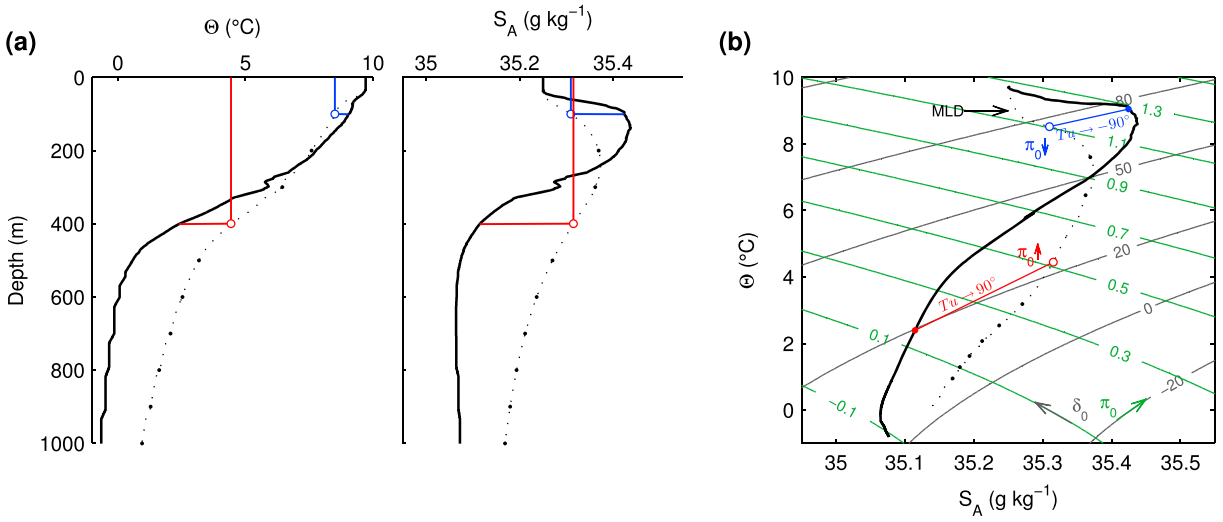

Figure 3. (a) Typical profile of temperature and salinity from the Svinøy section. The dotted line shows the evolution of the mixed layer properties with depth (black dots every 100 m). Two examples are shown in color for a MLD of 100 m (blue) and 400 m (red). (b) Same as Figure 3a but in the Θ/S_A space. MLD = mixed layer depth.

owing that $\alpha \mathrm{d}T \simeq \beta \mathrm{d}S$ along surface of constant density. Flament (2002) proposed an alternative definition only constrained by orthogonality to density surfaces ($\partial_T \pi . \partial_T \rho + \partial_S \pi . \partial_S \rho = 0$). Both definitions have density units and are numerically close. As noted by Flament (2002), a simple linear transformation gives a difference of less than 2.5% between the two definitions. Note that the Turner angle can be linked to the isopycnal gradient of spiciness: $Tu \sim -atan(\partial\pi/\partial\rho)$.

For sake of consistency and reproducibility, we use the most recent definition of spiciness by McDougall and Krzysik (2015), provided in the open-access Gibbs-Sea Water Oceanographic Toolbox. It follows the idea by Veronis (1972) and Munk (1981), and the definition of Jackett and McDougall (1985), but is adapted to the new standards of Absolute Salinity and Conservative Temperature. In addition, spiciness is constructed as a potential variable, hence not being affected by adiabatic heaving motions. Spiciness is here referenced at the surface (π_0), as we mainly focus on the AW.

2.5. Transformation of Spiciness by Vertical Mixing

To a large extent, spiciness can be considered as a passive variable, hence governed by horizontal advection and isopycnal mixing away from boundary layers. In surface mixed layers, it is importantly affected by turbulent mixing. Yeager and Large (2007) described a conceptual model of spiciness injection by vertical mixing describing how both temperature and salinity can increase along particular isopycnals. A necessary condition is the presence of density compensated temperature and salinity gradients in the water column (i.e., Turner angles between 45° and 90°). Then, when the mixed layer deepens under the action of cooling, a strongly density-compensated layer with high Turner angle is generated beneath the mixed layer in case of penetrative mixing. This has been particularly studied in subtropical oceans, where spicy waters are formed (e.g., Kolodziejczyk et al., 2015; Yeager & Large, 2004, 2007). In the Nordic Seas, warm and salty AW above cold and fresh deep waters sets up favorable conditions for spice injection, provided that winter mixing penetrates below the AW salinity maximum. Temperature indeed monotonically decreases with depth, while salinity gradient changes sign due to the presence of fresh surface waters.

As an example, let us consider a *T*-*S* profile characterized by a subsurface salinity maximum and monotonically decreasing temperature (Figure 3). The profile shown is typical of the AW properties at Svinøy section. The simple one-dimensional non-penetrative vertical mixing model by Lilly et al. (2003) is used to infer mixed layer properties (code freely accessible; Lilly, 2017). For simplicity, we assume zero precipitation minus evaporation, since surface cooling is the main driver of mixing in the Nordic Seas. Two contrasted examples illustrate the effect of vertical mixing on spiciness, as well as the generation of a density-compensated layer at its base. For shallow mixing, not reaching the depth of the salinity maximum, convection produces a water mass fresher and cooler compared to original water mass of same density. For deeper mixing, below the salinity maximum, the opposite effect is observed with increase in spiciness along isopycnals. In each case, the transition line joining the mixed layer to the initial profile tends to be parallel to isopycnals in the Θ/S_A space, meaning that

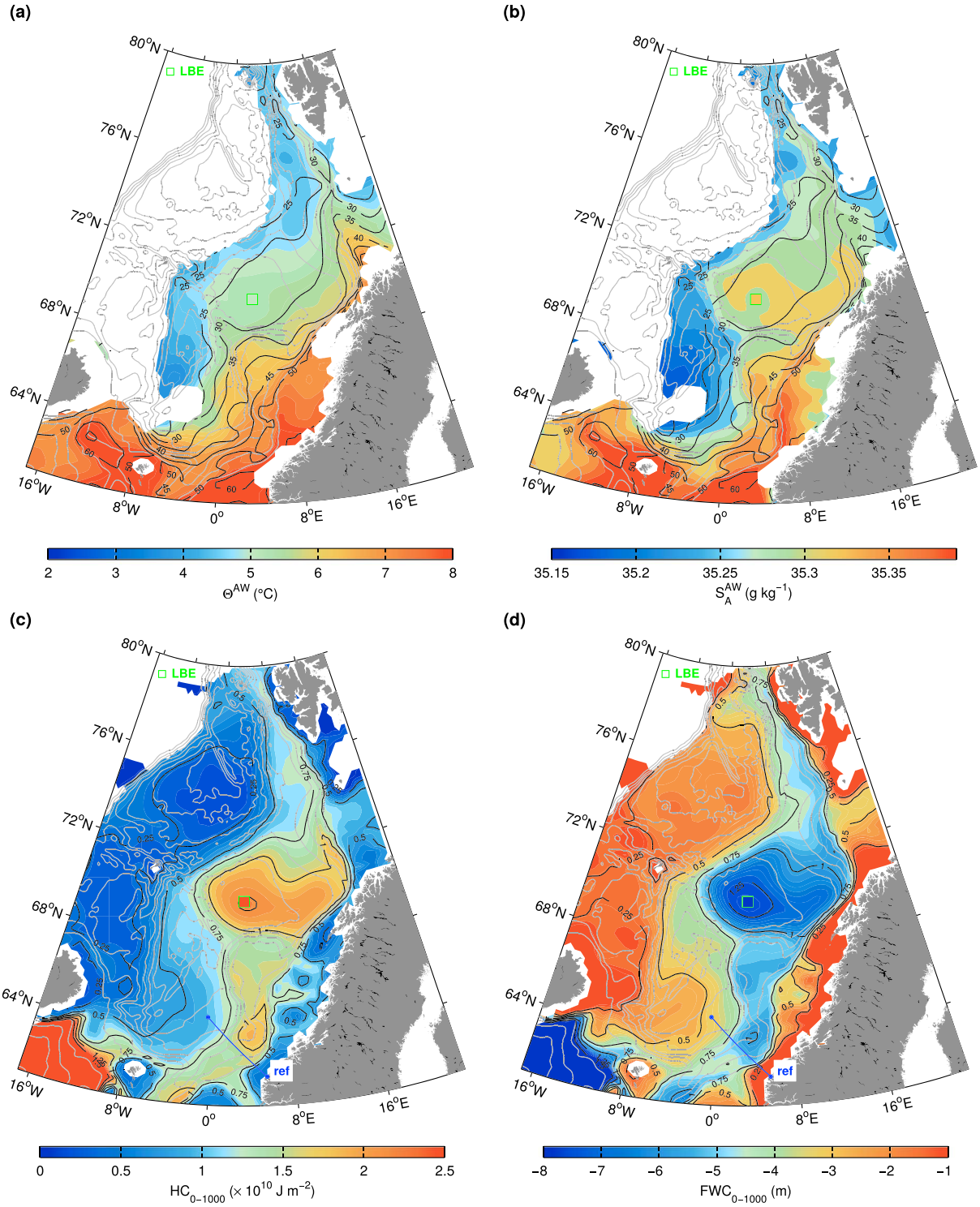

Figure 4. Objective map AW layer-averaged (a) conservative temperature, (b) absolute salinity, layer-integrated (c) heat, and (d) freshwater content to 1000 m (to the bottom in shallower areas). In (a) and (b), black contours show the mean specific volume anomaly of the AW. In (c) and (d), they show the ratio to the mean value at the Svinøy section (noted as *ref* on the map). The green square in the center of the Lofoten Basin shows values for the LBE: (a) 4.96 ± 0.06 °C, (b) 35.33 ± 0.01 g/kg, (c) 3.06 ± 0.11 × 10^{10} J/m^2 (1.74 times the value at Svinøy section) and (d) −11.67 ± 0.50 m (1.94 times the value at Svinøy section). Note that those latter numbers (c and d) for the LBE were integrated down to 1,500 m include the whole AW layer in its core. AW = Atlantic Water; LBE = Lofoten Basin Eddy; HC = heat content; FWC = freshwater content.

temperature and salinity gradients are strongly density compensated and Turner angle tends to 90° , in absolute value. As shown by Yeager and Large (2007), penetrative mixing allows strongly density compensated layers to extend below the mixed layer.

2.6. Optimal Interpolation

Variables are spatially interpolated using the following method. The considered field estimated for each profile is first bin averaged on a 25-km by 25-km grid, after excluding the LBE core and rim profiles. Note that for MLD (and its corresponding specific volume anomaly or PV), we consider the maximum (minimum) in each bin. This is done in order to represent a seasonal signal at its maximum amplitude. In a second step, the binned field is optimally interpolated using a covariance function $\mathrm{Cov}(D,F) = e + s\,\exp(-D^2/L^2 - F^2/\Phi^2)$, depending on the spatial distance D between binned observations, and their fractional distance F in f/h values, where f is the Coriolis parameter and h is the bathymetry. For two observations a and b, $F(a,b) = |f_a/h_a - f_b/h_b| / \sqrt{(f_a/h_a)^2 + (f_b/h_b)^2}$; see Boehme & Send, 2005, for details). The spatial correlation length scale L was set to 150 km with $\Phi = 1$ and the signal (respectively residual error) to $s = 0.9$ (respectively $e = 0.1$) of the variance. This represents the typical correlation at the basin scale. Relative errors are then used to mask data with interpolation error greater than 80% of the variance.

2.7. Definition of Regions

Regions of interest in Figure 1a are defined using the objectively analyzed AW properties (Figures 2a, 4, and 6).

1. The Svinøy section. This is a section that has been occupied since the 1950s by the Norwegian Institute of Marine Research (Mork & Blindheim, 2000). A reference state of AW entering the Nordic Seas during the study period is determined by isopycnally averaging profiles with AW thicker than 300 m along this section. Another reference for the AW inflow chosen at the Faroe-Shetland Channel led to slightly different numbers but similar patterns. The use of the Svinøy section is motivated by its high observational coverage crossing both branches of the AW circulation (NwASC and NwAFC).
2. The LB (area deeper than 2,750 m with δ_{21} exceeding 500 m). The basin is further divided into two parts showing different behaviors regarding winter mixing: the western part LB characterized by MLD exceeding 400 m and the eastern LB, influenced by eddies shed from the slope, exhibiting shallower mixing.
3. The NB (area deeper than 3,000 m with winter MLD larger than 250 m). This deep basin, bounded in the west by a southward flow of AW is known as an important region for vertical mixing (Latarius & Quadfasel, 2016).
4. BIW (area deeper than 2,000 m between 73 and 76°N with AW thickness exceeding 200 m). We will show that this area is important for AW transformation.
5. The WSC (area deeper than 250 m between 76.75 and 79.5°N with AW layer exceeding 150 m) and the BSO (71–76°N/18–23°E with AW thicker than 200 m). They are the two main exits from the Nordic Seas toward the Arctic.

3. Results

3.1. Poleward Evolution of AW

Along an isobar in the AW layer from the slope to the LB interior, temperature and salinity evolve toward 1.4 °C cooler and 0.06 g/kg fresher (and 0.14 kg/m^3 denser; see circle and cross at 250 m in Figure 2c). This difference illustrates the atmospheric winter cooling acting against the strong heat and salt input by the boundary circulation and the associated important cross-slope exchanges of heat and salt in the LB. To the northwest, AW is separated from the cold and fresh waters of the Greenland Sea by the Polar Front at the Mohn's Ridge. Little is known about cross-frontal exchanges occurring along this steep density front, despite its importance to close the heat and salt budgets of the basin (Segtnan et al., 2011).

The horizontal distribution of AW temperature and salinity in the Nordic Seas reflects important water mass modifications through air-sea interaction in winter (Figures 4a and 4b). While the mean AW temperature and salinity exhibit a general poleward decrease (especially marked between northern Norway and Svalbard), the LB stands out as a large heat and salt reservoir (Figures 4c and 4d). The thickening of the AW layer in the LB allows heat and salt to accumulate to values 25% above the reference Svinøy section. AW also becomes denser along the way. Density increases across the LB toward the Mohn's Ridge with a large area characterized by values between 25 and 30 $\times$ 10^{-8} m^3/kg, indicative of homogenization processes. North of 72°N, a strong cooling and densification of AW is also observed. It occurs in a region subjected to the largest heat losses in the Nordic Seas (e.g., Isachsen et al., 2007; Richards & Straneo, 2015), and downstream of the LB, where substantial transformation has already taken place.

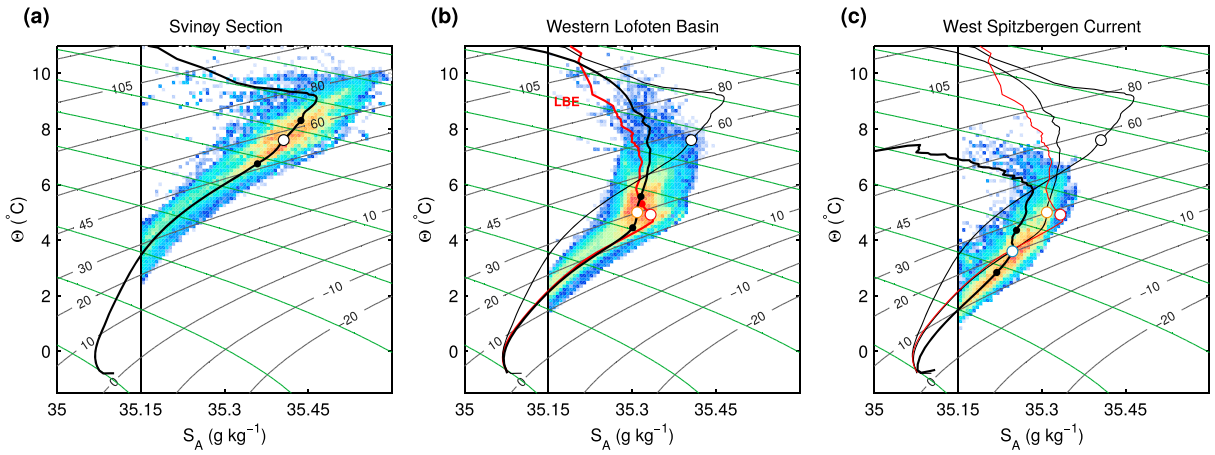

Figure 5. Θ/S_A diagram in different regions. Colors represent an arbitrary log scale of the number of counts for $S_A > 35.15$ g/kg (vertical line). Black lines indicate isopycnals in terms of specific volume anomaly (cubic meter per kilograms and multiplied by 10^8) and green ones are spiciness isolines spaced by 0.2 kg/m^3. In each panel, the thick solid black lines are mean profile averaged along isopycnals. Panel (b) shows in addition the mean profile in the LBE in red. To allow a quick comparison, light lines in panels (b) and (c) show mean profiles in upstream regions. The white dots are positioned at the median specific volume anomaly for $S_A > 35.15$ g/kg and the small black dots at the 25th and 75th percentiles (respectively for the Svinøy section: 48/56/63 $\times$ 10^{-8} m^3/kg, the deep LB: 25/30/36$\times$ 10^{-8} m^3/kg, the LBE: 27/28/33$\times$ 10^{-8} m^3/kg and the WSC: 16/20/27$\times 10^{-8}$ m^3/kg). LBE = Lofoten Basin Eddy.

The heat content of the upper 1,000 m of the water column is 1 order of magnitude smaller west of the Polar Front compared to the Atlantic sector (Figure 4c). The mean heat content at Svinøy section is $1.75(\pm 0.23)\times 10^{10}$ J/m^2. Compared to $1.03(\pm 0.31) \times 10^{10}$ J/m^2 in the WSC, 2 to 4 years would be required to release this heat to the atmosphere at an annual cooling rate of 50–100 W/m^2, typical of the Nordic Seas (e.g., Isachsen et al., 2007; Richards & Straneo, 2015). This also represents the average timescale for a water parcel to reach Fram Strait. In comparison, a fluid parcel advected at speed of the NwASC (0.1–0.3 m/s) would transit from the Svinøy section to Svalbard in a matter of months (3–9 months, considering a 2,400-km pathway). Lateral temperature and salt exchanges by eddies, however, are known to be important, especially in the LB (e.g., Andersson et al., 2011; Isachsen, 2015; Isachsen et al., 2012; Koszalka et al., 2011; Poulain et al., 1996; Rossby, Prater, & Søiland, 2009) and in the WSC (e.g., Boyd & D'Asaro, 1994; Hattermann et al., 2016; Nilsen et al., 2006). During the poleward advection of a water parcel, the reduction in heat content that cannot be accounted for by air/sea interaction is equivalent to a surface flux of 200–800 W/m^2. Along the boundary circulation, mesoscale eddies along with other lateral mixing processes flux heat toward the basin interior at a rate that largely overcomes air/sea fluxes.

The AW freshwater content increases northward, mainly through entrainment of fresh water of coastal origin. For example, the Norwegian Coastal Current carries fresh water from the Baltic Sea, continental runoff, and precipitation. In the LB, the shelf break is very close to the coast promoting interactions between the slope and coastal currents. Similarly around Svalbard, sea ice melt increases the freshwater content of the surface layer and can form a coastal current that can interact with the WSC. In the opposite, brine release from sea ice production on Svalbard's shelf can create salty and cold waters, dense enough to cascade downslope in Fram Strait (Quadfasel et al., 1988; Schauer, 1995). Freshening events can be linked to offshore Ekman transport of coastal waters by northerly winds (Nilsen et al., 2006). The observed increase in freshwater content of about 1.8 m between Svinøy and WSC is opposite to the slightly positive climatological air/sea fluxes and evaporation minus precipitation (order of 0.1 m/year; Isachsen et al., 2007). The freshwater content is thus mainly controlled by lateral exchanges rather than surface fluxes.

The LBE stands out as the largest heat and salt accumulation, reaching almost twice the values at Svinøy section (Figure 4). This anomaly is associated with the thickest AW layer of the Nordic Seas (about 1,200 m) characterized by warm (Θ ~4.9 °C) and salty ($S_A \sim 35.33$ g/kg) properties. This is consistent with the hypothesis that the LBE maintains its heat and salt anomaly by interacting with mesoscale anticyclones and absorbing their heat and salt transported from the slope (Köhl, 2007; Søiland & Rossby, 2013; Volkov et al., 2015). Deep convection in the LBE also plays a role in maintaining its large thickness of AW (Ivanov & Korablev, 1995a; Köhl, 2007).

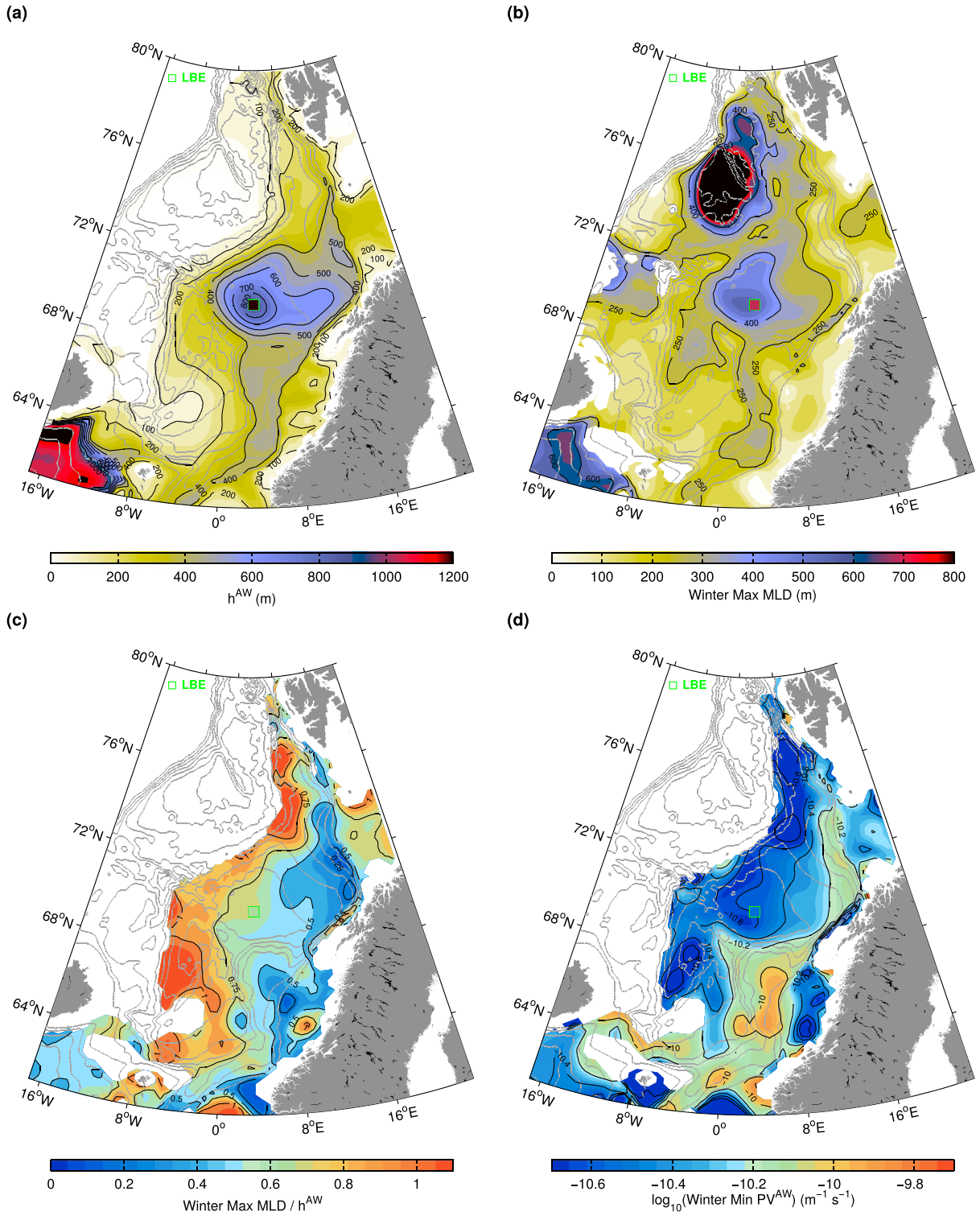

Figure 6. Objective maps of (a) AW thickness (h^{AW}), (b) winter maximum MLD, (c) ratio of winter maximum mixed layer to AW layer thickness, (d) winter minimum potential vorticity averaged in the AW layer (PV^{AW}). In all panels, the green squares show the values for the LBE: (a) $1,130 \pm 50$ m, (b) 690 ± 200 (this is the average of yearly maximum MLD, observations range from 1,130 m in 2010 to 490 m in 2015, in agreement with Yu et al., 2017), (c) 0.67 ± 0.17 and (d) $\log_{10}(PV) = -10.77 \pm 0.06$ m/s). AW = Atlantic Water; MLD = mixed layer depth; LBE = Lofoten Basin Eddy; PV = potential vorticity.

3.2. AW Modification in the Θ/S_A Space

The evolution of AW properties in the Θ/S_A space shows that AW becomes colder, fresher, and denser from the Svinøy section to the LB and finally to the WSC (Figure 5). At Svinøy, warm and salty inflow of AW is characterized by $\Theta \sim 7.6$ °C, $S_A \sim 35.41$ g/kg, $\delta \sim 56 \times 10^{-8}$ m^3/kg (or $\sigma_0 \sim 27.5$ kg/m^3). In the LB, particularly in the western and deepest part of the basin, AW becomes substantially colder by −2.6 °C and fresher by −0.1 g/kg, corresponding to an increase in density ($\delta \sim 30 \times 10^{-8}$ m^3/kg or $\sigma_0 \sim 27.8$ kg/m^3). Eventually, at the northernmost part of the Nordic Seas in the WSC, AW is cooled down further by −1.4 °C and freshened by −0.06 g/kg compared to the LB, with again an increase in density ($\delta \sim 20 \times 10^{-8}$ m^3/kg or $\sigma_0 \sim 27.9$ kg/m^3). F5

Between the Svinøy section and the LB, the cooling of the AW clearly dominates over freshening, with a density ratio $R_\rho = \alpha\Delta\Theta/\beta\Delta S_A \sim 4.8$, with the density change given by $\Delta\rho = \beta\Delta S_A(1 - R_\rho)$. The ratio α/β is evaluated for the average AW temperature, salinity, and pressure of the two considered regions. By definition, R_ρ is unity when mixing purely occurs along isopycnals without change in density. This would be expected for eddy-driven lateral mixing of two water masses of same density but different Θ/S_A properties (i.e., different spiciness). In the energetic Nordic Seas, the large density ratio highlights the importance of surface heat loss and vertical mixing in the water mass transformation. In the LBE R_ρ peaks at 6.7, indicating different isopycnal and vertical mixing conditions in this permanent eddy compared to the basin. The transformation from the LB to the WSC still remains dominated by surface heat flux with $R_\rho \sim 3.4$.

In the LB, isopycnals between 25 and 35×10^{-8} m^3/kg constitute most of the AW layer. Compared to Svinøy along $\delta = 30 \times 10^{-8}$ m^3/kg, AW in the LB is warmer (+0.95 °C) and saltier (+0.13 g/kg). In the LBE, along $\delta = 28 \times 10^{-8}$ m^3/kg, the warming (+1.28 °C) and salinification (+0.17 g/kg) is even higher. A similar feature is also observed in the WSC with an increase in temperature and salinity of, respectively, 1.05 °C and 0.12 g/kg, along a deeper isopycnal typical of AW density in that region ($\delta = 20 \times 10^{-8}$ m^3/kg). This reflects a clear and important increase in spiciness along deep isopycnals from Svinøy section to Fram Strait.

3.3. Winter Convection in the Nordic Seas

There is a distinct region in the western part of the LB where MLD exceeds 400 m, with a maximum of about 500 m in the deepest part of the basin (Figure 6a). Elsewhere in the Nordic Seas, winter MLD only reaches 200 to 300 m. The deepest mixed layers are observed in the Greenland Sea, where the water column is preconditioned to open-ocean deep convection by a basin-scale cyclonic circulation (Marshall & Schott, 1999) and the AW transformation on the way north. Considering only the Norwegian Sea (i.e., the warm Atlantic sector), winter convection is the deepest in the LBE core with, on average, a maximum winter MLD exceeding 800 m during the study period (absolute maximum of 1,130 m observed in winter 2010). In the recent period (2013–2017), gliders have observed shallower MLD in the LBE sleading to formation of intermediate pycnoclines, further preventing the mixing from reaching the base of the AW (Yu et al., 2017). F6

Although winter buoyancy loss in the LB is higher than in the Greenland Sea (Richards & Straneo, 2015; Segtnan et al., 2011), a strong pycnocline at the base of the AW prevents vertical mixing to penetrate deeper. The ratio of winter MLD to the AW layer thickness is a proxy for the intensity of the AW mixing (Figure 6c). This ratio is high in the western part of the Atlantic sector, away from the boundary circulation, where more than three quarters of the AW are affected by vertical mixing. This ratio is close to unity in the NB and BIW between the two branches of Atlantic currents. The AW and mixed layer in those regions are both approximately 250-m thick.

The vertical mixing intensity is manifested in the PV of the AW layer (Figure 6d). When the mixed layer approaches the base of AW, its PV is significantly lowered, as the density gradient between the AW and the underlying intermediate waters is reduced. This mechanism is particularly pronounced in the western LB, where strong modifications of AW occur. Farther downstream toward Fram Strait, the modified AW is easier to mix, and deeper isopycnals at the base of the AW can outcrop in winter. The AW finally flowing poleward in Fram Strait is strongly affected by mixing west of Bear Island and Svalbard, where the whole AW layer is convected and the AW stratification is reduced. On the contrary, mixing does not penetrate deep enough in the eastern LB to significantly reduce the PV of AW. Convection reaches only about half or less of the AW thickness, impeded by restratifying lateral buoyancy fluxes from the slope.

3.4. Spice Injection by Winter Diapycnal Mixing

The densest outcropping isopycnal in winter shows values of δ ranging from 25 to 35×10^{-8} m^3/kg in the western LB (Figure 7a). Denser isopycnals outcrop in the NB (21–31×10^{-8} m^3/kg), as well as west of Bear Island

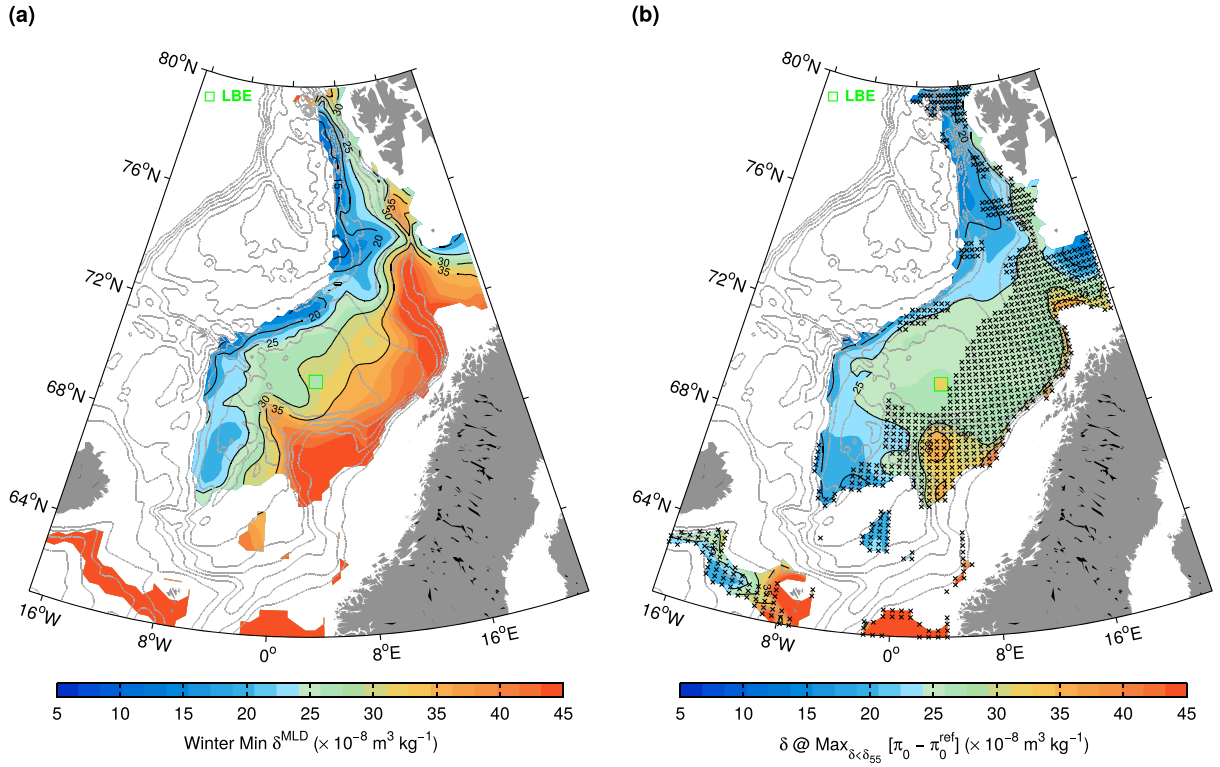

Figure 7. (a) Winter minimum specific volume anomaly averaged over the mixed layer depth. (b) Specific volume anomaly of the maximum spiciness injection. Crosses indicate where the winter minimum mixed layer specific volume differs from that of the maximum spiciness injection by more than 5×10^{-8} m^3/kg. The green squares show values observed in the LBE, respectively, 27 ± 2 and $27 \pm 5 \times 10^{-8}$ m^3/kg. Note that thin AW layers ($h^{AW} < 100$ m, from Figure 6a) or spiciness injection smaller than 0.05 kg/m^3 have been masked out. LBE = Lofoten Basin Eddy; AW = Atlantic Water.

and Svalbard ($17-27\times10^{-8}$ m^3/kg). Different density classes are thus affected by vertical mixing in these three regions, with different mean AW density. Anomalies along isopycnals relative to the Svinøy reference show an increase in spiciness on Θ/S_A diagrams (Figure 5). Below the surface layer ($\delta > 55 \times 10^{-8}$ m^3/kg equivalent to $\sigma_0 < 27.5$ kg/m^3), the isopycnal with maximum spiciness increase can further be compared with outcropping isopycnals (Figure 7b). Crosses mask out areas where δ in the mixed layer differs from that of the maximum spiciness increase by more than 5×10^{-8} m^3/kg. In the entire eastern LB, as well as in the BSO, vertical mixing is limited to density levels shallower than where spiciness is injected. Thus, the spiciness increase cannot be locally generated and must be explained by lateral advection from a remote location. On the other hand, winter vertical mixing matches spiciness injection in the density space in the NB, in the western LB, and LBE, as well as farther downstream toward Fram Strait.

Isopycnals denser than about 45×10^{-8} m^3/kg (35×10^{-8} m^3/kg in the NB) exhibit spiciness injection (positive large values), with a peak at 25×10^{-8} m^3/kg in the western LB and LBE (Figure 8a). In the WSC, the spiciness injection peaks at a denser level, but with a smaller amplitude. However, in contrast to NB and LB, the spiciness injection in the WSC reaches much denser waters, down to 10×10^{-8} m^3/kg. The BSO shows a pronounced increase of spiciness in the deepest levels, almost exceeding the signal in the LB. The source of this spiciness is likely not linked to the water mass transformation in the Nordic Seas but to that in the Barents Sea and the properties of the deep outflow from the Barents Sea to the Norwegian Sea through the northern BSO (Århun et al., 2011; Furevik, 2001).

PV can be used to track waters affected by winter convection. Interestingly, a layer with PV minimum is centered around the maximum spiciness injection, providing further evidence for the link between vertical mixing and the spiciness injection (Figure 8b). Moreover, these layers with low PV and high spiciness have a density similar to the density of winter mixed layer in these regions (vertical bars in Figure 8b). Around $\delta = 15 \times 10^{-8}$ m^3/kg, a PV maximum corresponds to the strong stratification at the base of AW. The PV of this layer is notably reduced in the northern part, particularly in BIW and to a lesser extent in the NB, as mixing penetrates into denser layers.

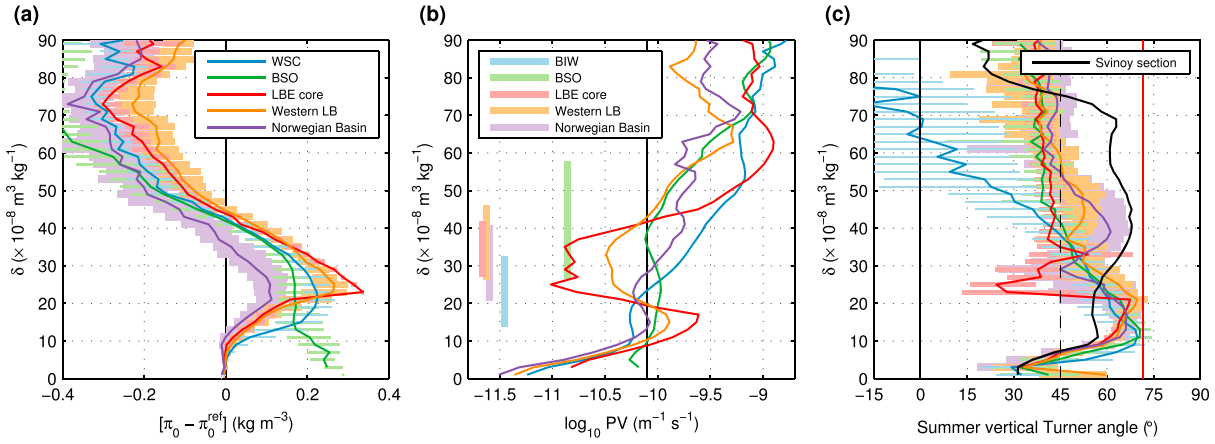

Figure 8. (a) Isopycnal spiciness difference with Svinøy section in different regions. Lines represent the median value, and bars the 25th and 75th percentiles in each interval. (b) Median potential vorticity averaged along isopycnals in different regions. Vertical bars show the minimum PV and range of specific volume anomaly observed in winter mixed layer (represented by the 25th and 75th percentiles of specific volume anomaly observed in winter mixed layers). (c) Vertical Turner angle binned in isopycnal layers. Lines represent the median value and bars the 25th and 75th percentiles. Colors are identical to (a) with in addition the Svinøy section shown in black. The vertical red line represents the threshold of salt-fingers growth ($Tu > 71.6°$). PV = potential vorticity; WSC = West Spitsbergen Current; BSO = Barents Sea Opening; LBE = Lofoten Basin Eddy; LB = Lofoten Basin.

Spiciness injection is observed where the vertical Turner angle typically exceeds 45° (Figure 8c). Note that only summer profiles are considered, because *Tu* is too noisy in the winter mixed layer. Spiciness injection by vertical mixing should also impact the temperature and salinity gradients in the transition layer, at the base of the mixed layer (Yeager & Large, 2007) . In deeper layers below the spiciness increase, *Tu* reaches 70° on average, indicating strongly density-compensated temperature and salinity gradients. These values are close to the critical value for salt-fingering instability ($Tu > 71.6°$ or $R_\rho < 2$; Schmitt & Evans, 1978), especially in the WSC where *Tu* is the highest. This could have important implications, as AW is about to reach the Arctic Ocean, where double diffusion has time to develop (Rudels et al., 1999). From the Svinøy section, there is a clear poleward increase in the Turner angle within layers between 10 and 20×10^{-8} m^3/kg. In the BSO, the lack of *Tu* increase associated with the deep spiciness injection supports the idea that this signal is generated remotely in the central Barents Sea, where bottom waters can be formed (Loeng, 1991). The transition layer would then be absent, and the Turner angle increase suppressed.

3.5. An Isopycnal Analysis of Spiciness

The increase in spiciness caused by convective mixing has typical values of 0.21(±0.06) kg/m^3 in the LB and WSC and up to 0.31(±0.03) kg/m^3 in the LBE. In the LB, this corresponds to a substantial increase in temperature of 1.14(±0.28) °C and in salinity of 0.15(±0.04) g/kg (Figures 9a and 9b). Farther north toward Fram Strait, similar values are observed in the WSC. In the LBE, the spiciness increase is the largest, associated with an increase in temperature and salinity reaching 1.48(±0.20) °C and 0.20(±0.02) g/kg. The spiciness injection is discontinuous across the continental slope toward BSO, implying a different origin for the spiciness in the BSO, confirming our previous interpretation. Finally, the spice injection in the NB is less pronounced than in the LB and farther north with an increase of only 0.12(±0.06) kg/m^3 (Θ and S_A increase of 0.64(±0.30) °C and 0.08(±0.04) g/kg).

Apart from a thin surface layer, a large part of the AW in the LB is impacted by the convectively generated spiciness increase (Figure 9c). The winter mixed layer δ (black bars in Figure 9c) can be compared to that of the maximum spiciness injection, centered at about $\delta = 25\times10^{-8}$ m^3/kg. Winter mixing injects spiciness to deep isopycnals in the western LB, whereas it does not reach deep enough in the eastern LB to explain the observed spiciness. Even the deep spiciness injection in the LBE is limited to comparable isopycnals as in the eastern LB. The spiciness increase spreads over the whole LB in deep isopycnals (δ between 20 and 35×10^{-8} m^3/kg) and must originate from the western LB where the winter mixing and spiciness injection coincide in density space. Then, along-isopycnal spreading driven by the vigorous mesoscale field of the LB could explain the connection toward east, where the spiciness signal slightly decreases but remains substantial. While bringing heat and salt to the LB and feeding the mesoscale field, buoyant eddies shed from the boundary current thus

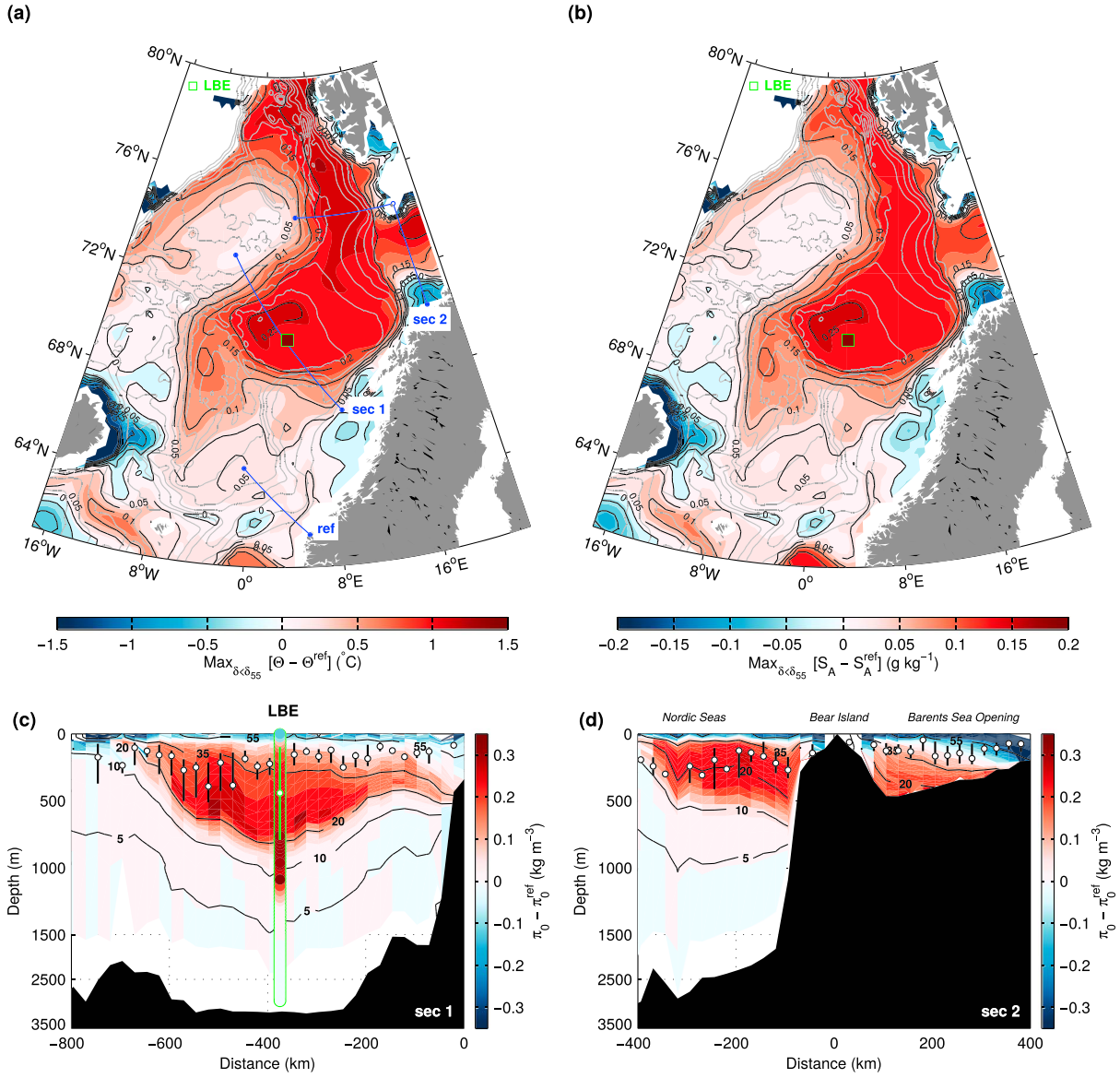

Figure 9. Maximum along isopycnal anomaly of (a) conservative temperature and (b) absolute salinity relative to the Svinøy section for $\delta < 55 \times 10^{-8}$ m^3/kg (to exclude the surface waters). In both (a) and (b), black contours show the corresponding spiciness increase (cubic meter per kilograms). The green squares show the values observed in the LBE. Distribution of isopycnal spiciness difference relative to the reference for (c) section 1 and (d) section 2. Black contours are specific volume anomaly, and black bars show the winter mixed layer characteristics (white dots are median, thick lines drawn between the 25th and 75th percentiles). Section 1 crossing the Lofoten Basin separately shows the signal in the LBE (as in Figure 2). LBE = Lofoten Basin Eddy.

also play an important role in the eastward advection of spiciness in deep isopycnals. The modified AW can thereby be incorporated into the boundary circulation and continue its poleward transit.

A section extending west of Bear Island shows a significant spiciness increase in deeper isopycnals than in the LB, down to $\delta = 10 \times 10^{-8}$ m^3/kg (Figure 9d). Spiciness can be used as a tracer of the horizontal circulation and shows continuous values from the western LB to BIW. However, the strongest spiciness injection progressively moves to denser isopycnals toward Fram Strait (Figure 7a). This can be the result of local air-sea interaction (Figure 7b). Winter mixing west of Bear Island (and to a lesser extent downstream in the WSC) indeed occurs at δ levels ranging from 15 to 25×10^{-8} m^3/kg, matching the shift observed in spiciness injection.

The isopycnal spiciness analysis is repeated using a reference chosen in the western LB, instead of Svinøy (Figure 10a). While the layer already transformed in the LB remains similar, the spiciness increases along denser isopycnals between 10 and 20 $\times 10^{-8}$ m^3/kg (i.e., 27.9 $< \sigma_0 <$ 28 kg/m^3). Most of this increase appears

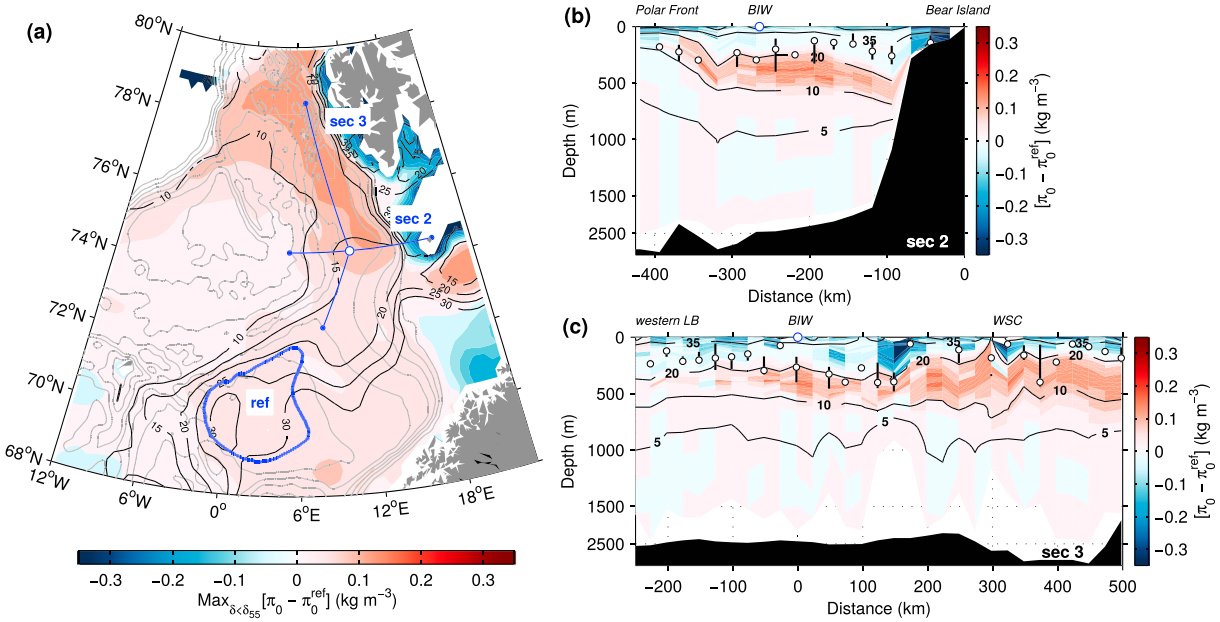

Figure 10. (a) Same as Figure 9a but for spiciness anomaly from a reference state in the western LB (inside the blue line). Contours represent the specific volume anomaly at the maximum spiciness anomaly ($\times 10^{-8}$ m^3/kg). Panels (b) and (c) are similar to Figures 9c or 9d but with the reference state in the western LB. The location of the two sections is shown in (a). LB = Lofoten Basin; BIW = Bear Island West; WSC = West Spitsbergen Current.

between 73 and 75°N, close to the mid-ocean ridge, and then in the northernmost part of the WSC with a thickening of the layer between 10 and 20 $\times 10^{-8}$ m^3/kg. The winter mixed layer δ there is comparable to that of spiciness injection west of Bear Island (Figures 10b and 10c), suggesting that winter vertical mixing can be its source. Keep in mind that winter observations of mixed layer in these areas remain sparse. As in the LB, the deepest spiciness injection occurs in the vicinity of the Polar Front about 150–200 km away from the boundary circulation and its restratifying influence. This is also where PV is strongly reduced in winter (Figure 6d). The NwAFC likely plays an important role in transferring the strongly modified AW from the western LB to Fram Strait, while it undergoes additional transformations along the way. It is worth noting that spiciness signal of the transformed AW also spreads toward Greenland, in the recirculating branch of AW in Fram Strait, and farther west and south with the East Greenland Current (Hattermann et al., 2016; Manley, 1995).

3.6. Volume of AW Transformation

The volume of AW involved in the spiciness injection can be inferred from climatological maps. The formation of low PV layers, in a process similar to the formation of a *mode water*, is closely linked to spiciness transformation. Based on a criterion on spiciness injection relative to a certain reference (>0.05 kg/m^3), we estimate the volume of AW modified, at least once, by winter mixing downstream of that reference. To avoid a potential bias due to seasonality, only summer profiles are considered here. Dividing the Nordic Seas into three main basins, volume of enhanced spiciness is 1.7×10^{14} m^3 (equivalent to about 5.4 Sv) in the LB, 1.5×10^{13} m^3 (0.5 Sv) in the NB and 2.7×10^{13} m^3 (0.9 Sv) west of Bear Island and Svalbard (reference in the western LB).

On the other hand, the area of outcropping isopycnals fitting those of maximum spiciness injection (non-crossed area in Figure 7b) multiplied by the winter MLD (Figure 6b) provides an estimate of the volume of convected waters. It represents the mean state during the study period of seasonal spiciness injection: 1.5×10^{13} m^3 (0.5 Sv) in the NB, 5.8×10^{13} m^3 (1.8 Sv) in the LB, and 2.7×10^{13} m^3 (0.8 Sv) west of Bear Island and Svalbard. These numbers are consistent with volumes of annual mean surface transformation estimated by Isachsen et al. (2007) over the whole Nordic Seas of about 3–5 Sv for potential density between 27.8 and 27.9 kg/m^3 (roughly corresponding to 20 to 30 $\times 10^{-8}$ m^3/kg).

This approach neglects the interannual variability of winter mixing and spice injection. Moreover, as we considered the distribution of the maximum observed MLD, the volume of convected waters should be an upper bound. Winter convection is thus able to renew about one third of the enhanced spiciness volume observed in the LB, 95% of it west of Bear Island and Svalbard, as well as in the NB. One can thus expect a rapid advection of the deep spiciness anomaly in different basins on a seasonal timescale or slightly more in the LB.

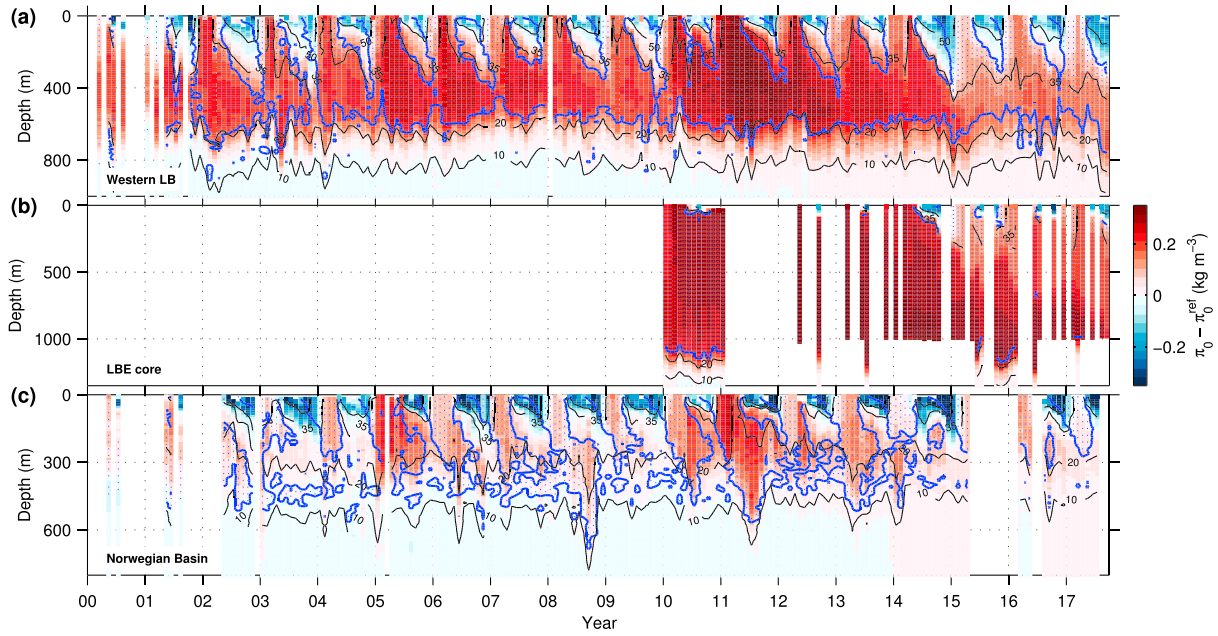

Figure 11. Spiciness difference with Svinøy in the depth time space in (a) the western LB, (b) the LBE core, and (c) the NB. The data are binned in 1 month and 10-m intervals. The blue contoured and dotted area shows the weakly stratified waters with PV lower than 8×10^{-11} m/s (i.e. , $\log_{10}(PV) < -10.1$). Black contours represent isopycnals at δ = 10, 20, 35, and 50 $\times 10^{-8}$ m^3/kg. LB = Lofoten Basin; LBE = Lofoten Basin Eddy; NB = Norwegian Basin.

3.7. Interannual Variability of AW Transformation

The low PV layer formed in winter delineates the increase of spiciness in the LB, LBE, and NB, where the data coverage enables a seasonal description (Figure 11). It confirms that spiciness injection is maximum where PV is reduced by winter vertical mixing. Interestingly, even if the spiciness injection is restricted to a narrow range of isopycnals, it expands to most of the AW layer, apart from a surface layer found in summer and characterized by negative spiciness anomaly. A thin surface layer of fresh and warm waters from the shelf usually spreads offshore during summer. Its offshore advection, observed in 2014 to the western part of the LB and the LBE, could play an important role in the freshwater budget and needs a closer investigation beyond the scope of this study. Northerly wind anomalies have already been identified as a potential cause for freshwater intrusions at the offshore Ocean Weather Station M (66°N, 2°E) by Nilsen (2006).

In the LBE, the spiciness anomalies span over the top 1,200 m of the AW with a lesser influence of summer intrusions of fresh surface waters compared to the LB. A maximum of spiciness is reached in winter 2012 and

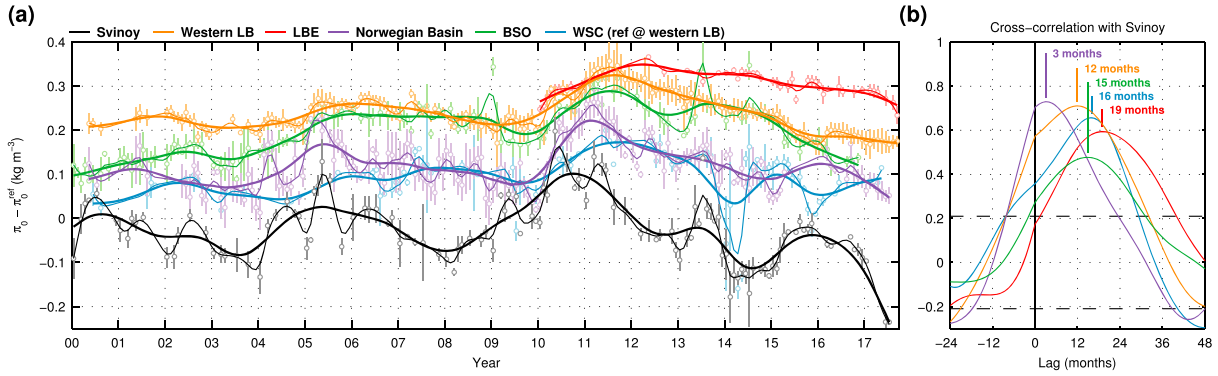

Figure 12. (a) Temporal evolution of the spiciness difference relative to the reference state. At the Svinøy section, the gray dots represent the spiciness anomaly averaged between 35 and 55$\times 10^{-8}$ m^3/kg and the gray bars the standard deviation. The light and thick curves are low-pass filtered with a 3- and 12-month cutoff, respectively. For other regions, dots are the 95th percentile between 15 and 35$\times 10^{-8}$ m^3/kg. (b) Cross-correlation function of the low-frequency spiciness evolution with that of the other regions. The dashed line indicates bounds of significance. LB = Lofoten Basin; LBE = Lofoten Basin Eddy; BSO = Barents Sea Opening; WSC = West Spitsbergen Current.

persists for several years below about 800 m. From winter 2013 to 2017, the vertical mixing in the LBE did indeed not reach deeper than 800 m (Yu et al., 2017), allowing for the deepest part of the LBE core with the strongest spiciness injection to stay isolated. This confirms the importance of winter convection for LBE regeneration in deep layers. The evolution of this core was thus governed by internal mixing processes associated with multiyear timescales (Fer et al., 2018). Interestingly, the spiciness reduction observed from 2011 seems to be less marked in the LBE than in other regions (Figure 12a) that can be explained by the presence of the spicy waters formed in 2012 and isolated at depth.

In the WSC, remarkably low spiciness anomalies appear in spring 2014 and 2016 and last for a few months (Figure 12a). It corresponds to intrusions of dense waters formed on the Svalbard's shelf characterized by anomalously cold characteristics along isopycnals where spiciness is enhanced by offshore vertical mixing ($10-25\times10^{-8}$ m^3/kg). Similarly, spiciness in the BSO generally follows the signal generated in the LB with a few months lag and a smaller amplitude. Peaks of spiciness injection in particular years (2009, 2013, and 2014, for instance) likely result from dense water mass formed in the central Barents Sea. The flow west of Svalbard has a complex behavior influenced by the main Atlantic currents, as well as local water mass production and the Barents Sea outflow during particular years.

The AW inflow spiciness at Svinøy shows interannual and seasonal variability (Figure 12a). The seasonal cycle is seen at the Svinøy section and in the Norwegian and LBs (thin lines in Figure 12a). On longer time scales, the inflowing AW spiciness peaks after winter 2005 and 2010. These maxima correspond to the highest salinity and temperature values observed since the 1960s, as reported by Holliday et al. (2018). These two local maxima led to a strong increase in the spiciness injection in other basins during winters 2005 and 2010–2011. This latter period of high spiciness shows also particularly intense convection (especially in 2011). The presence of salty AW could impact winter mixing by reducing the stratification. Warmer AW could strengthen air-sea temperature gradients, hence the heat loss to the atmosphere, and favor vertical mixing. In 2014, the inflow at Svinøy reached a local minimum in spiciness followed about 1.5 years later by a decrease in spiciness in the western LB and farther to the WSC. From 2011 on, there is an evolution toward less spicy AW flowing at Svinøy, as well as a decrease in the density reached by winter mixing in the LB, despite no clear evolution observed in the mixing depth. There is a clear decrease in the outcropping density after 2015 (Figure 11a). In 2017, the practical salinity at 100 m measured at Svinøy section has decreased to values as low as 35.15, corresponding to values comparable to the *great salinity anomaly* events (Dickson et al., 1988; Belkin et al., 1998).

There is a strong correlation between the spiciness at Svinøy and that of the modified AW in other regions (Figure 12b). A cross correlation of the low-frequency spiciness signals referred to the Svinøy time series yields the following lags: 3 months for the NB, 12 months for the deep LB, 15 months for the BSO, 16 months for the WSC, and finally 19 months for the LBE. Surprisingly, the largest lag is associated with the LBE. The inflowing waters into the Nordic Seas thus take more time to reach to the LBE core than Fram Strait. A direct advection speed of the signal from Svinøy to the western LB yields a speed of 2.4 cm/s, slightly less than the rate of advection toward the WSC (3.5 cm/s). This is coherent with the advection speed of freshwater signals during the great salinity anomaly events (Dickson et al., 1988). To reach the deepest part of the LB (and possibly interact with the LBE), spiciness anomalies need to be transported by eddies, whose movement is wiggly and slower than boundary currents ((Richards & Straneo, 2015) estimated it to about 6 cm/s in the LB).

4. Summary and Discussion

We describe the transformation of AW in the Nordic Seas from an isopycnal point of view, with particular attention on the role of the LB in transferring temperature and salinity (i.e., spiciness) signals toward dense layers. Deep mixing reaching the base of AW occurs in the western part of the basin injecting spiciness within a specific range of isopycnals. By definition, spiciness can be used as a tracer of the ocean circulation. The signal of spiciness is observed over the entire basin, even at depths not reached by winter mixing. Horizontal spreading must thus play an important role. There is a dynamical separation in the LB, set by two competing processes acting on the water column stratification. On the one hand, atmospheric fluxes drive intense heat loss over the basin. On the other hand, buoyant eddies shed from the boundary circulation drive restratification and a westward cross-slope flux of heat and salt. We show here that the eddy field is also responsible for an eastward flux of the enhanced spiciness observed along deep isopycnals in the western LB. The Polar Front might play an important role in connecting the western LB to the regions farther north, to Fram Strait. Strong air-sea interactions generate a secondary spiciness injection into denser isopycnals in the vicinity of

the frontal Atlantic currents. An upper bound of AW convection in the Nordic Seas is estimated to be 3.1 Sv (1.8 Sv in the LB, 0.5 Sv in the NB, and 0.8 Sv west of Bear Island and Svalbard), which is comparable to the volume of waters showing an increased spiciness. The advection timescale of spiciness anomalies from the inflow at the Svinøy section to the LB, where it impacts spiciness injection, is approximately 12 months. Three to six months later, the signal reaches the regions connecting the Nordic Seas to the Arctic (WSC and BSO), consistent with the mean circulation being coupled to strong lateral exchanges, driven by the mesoscale field. The LBE, a permanent anticyclonic eddy located in the basin center, exhibits the strongest spiciness injection and a longer time lag, hence a memory effect. This is a signature of the eddy's important retention.

The described mechanism of spice injection in the Nordic Seas plays an important role in building up the large heat and salt content anomaly of AW in the LB (and LBE). The deep winter convection in the western LB leads to the formation of thick, weakly stratified layers with increased temperature and salinity, with an annual production rate of up to 1.8 Sv. This can be used as a guideline for numerical models. Reasonable patterns of winter mixing in the LB should help to represent realistic heat and salt contents in the Nordic Seas. Moreover, the propagation of AW thermohaline anomalies in a strongly coupled ocean-atmosphere system can have further consequences for the climate prevailing over northwestern Europe. A substantial amount of AW entering the LB is transformed by diapycnal mixing into low stratified waters that can be qualified as a mode water. It may further have influence on biogeochemical tracers such as nutrients, dissolved oxygen, and the different components of the carbonate system. Vertical mixing acting against horizontal restratification from the slope forms contrasted dynamical regimes from east to west of the LB, with impacts on ocean ventilation. Further consequences are expected regarding phytoplankton blooms' timing and intensity, as well as on the subsequent ocean carbon uptake. The quick horizontal spreading of spiciness signals suggests that other tracers might follow a similar pattern. As weakly stratified AW transformed in the LB spreads northward, it can help preconditioning winter mixing to reach deeper and denser levels west of Bear Island and Svalbard. The role of the Polar Front in the advection of modified AW to Fram Strait remains to be investigated. Instabilities of the WSC interacting with the well-mixed AW layer observed offshore could significantly contribute to its important cooling rate. Finally, spice injection also affects the vertical structure of AW, with the formation of strongly density-compensated layers. The base of the AW is then characterized by high Turner angles, close to values favorable for development of double-diffusion processes. Spice injection ultimately defines the thermohaline properties of AW exiting the Nordic Seas with potential important consequences for the Arctic Ocean heat budget and for the sea ice.

Various important processes contributing to the variability and propagation of AW in the Nordic Seas are affected by multiyear variability. Important questions remain about the fate of the AW in our changing climate with warming oceans and a reduced sea ice cover in the Arctic. Trends have been reported on the decrease of deep convection intensity in the Greenland Sea or the numerous impacts of the sea ice decline in the Barents Sea. Coupled ocean-atmosphere numerical studies could be used to shed light on the spiciness evolution in the Nordic seas in the context of interannual variability and climate change, identify potential impact on the thermohaline circulation, and further quantify the atmospheric response to ocean circulation changes. In general, combining the analysis of mixed layer properties and spiciness is a useful tool to study water mass transformation. Winter mixed layer shows where spiciness can be injected (or removed). Tracking spiciness anomalies further reveals how and where they spread. A similar approach could be fruitfully applied to other convective basin with strong air-sea interaction like the Greenland and Iceland Seas in the Nordic Seas, the Labrador and Irminger Seas in the North Atlantic, the Southern Ocean, or the Mediterranean Sea. It could help better identify patterns of circulation and their potential evolution in the context of climate change.

Acknowledgments
ICES hydrographical profiles can be freely downloaded (http://ocean.ices.dk/). The Norwegian Marine Data Center also provides online access to its database (https://nmdc.no/datasett) and specifically to delayed mode data from the Seaglider missions in the Lofoten Basin (https://doi.org/10.21335/NMDC-UIB.2017-0001). Profiles from Argo floats were collected and made freely available by the Coriolis project and programs that contribute to it (http://www.coriolis.eu.org). These data were collected and made freely available by the International Argo Program and the national programs that contribute to it (http://www.argo.ucsd.edu, http://argo.jcommops.org). The Argo Program is part of the Global Ocean Observing System. This study received funding from the Research Council of Norway, through the project *Water mass transformation processes and vortex dynamics in the Lofoten Basin of the Norwegian Sea (PROVOLO)*, project 250784.

References

Alexeev, G. V., Bagryantsev, M. V., Bogorodsky, P. V., Vasin, V. B., & Shirokov, P. E. (1991). Structure and circulation of water masses in the area of an anticyclonic vortex in the northeastern part of the Norwegian Sea [in Russian]. Russian Problems of Arctic and Antarctic, 65.

Andersson, M., Orvik, K. A., LaCasce, J. H., Koszalka, I., & Mauritzen, C. (2011). Variability of the Norwegian Atlantic Current and associated eddy field from surface drifters. *Journal of Geophysical Research*, *116*, C08032. https://doi.org/10.1029/2011JC007078

Argo (2000). Argo float data and metadata from Global Data Assembly Centre (Argo GDAC). SEANOE. https://doi.org/10.17882/42182

Årthun, M., Eldevik, T., Smedsrud, L. H., Skagseth, Ø., & Ingvaldsen, R. B. (2012). Quantifying the influence of Atlantic heat on Barents Sea ice variability and retreat. *Journal of Climate*, *25*(13), 4736–4743. https://doi.org/10.1175/JCLI-D-11-00466.1

Årthun, M., Eldevik, T., Viste, E., Drange, H., Furevik, T., Johnson, H. L., & Keenlyside, N. S. (2017). Skillful prediction of northern climate provided by the ocean. *Nature Communications*, *8*, 15875. https://doi.org/10.1038/ncomms15875

Årthun, M., Ingvaldsen, R. B., Smedsrud, L. H., & Schrum, C. (2011). Dense water formation and circulation in the Barents Sea. *Deep-Sea Research Part I: Oceanographic Research Papers*, *58*(8), 801–817. https://doi.org/10.1016/j.dsr.2011.06.001

Belkin, I. M., Levitus, S., Antonov, J., & Malmberg, S.-A. (1998). "Great Salinity Anomalies" in the North Atlantic. *Progress in Oceanography*, *41*(1), 1–68. https://doi.org/10.1016/S0079-6611(98)00015-9

Beszczynska-Möller, A., Fahrbach, E., Schauer, U., & Hansen, E. (2012). Variability in Atlantic water temperature and transport at the entrance to the Arctic Ocean, 1997–2010. *ICES Journal of Marine Science*, *69*(5), 852–863. https://doi.org/10.1093/icesjms/fss056

Beszczynska-Möller, A., Woodgate, R., Lee, C., Melling, H., & Karcher, M. (2011). A synthesis of exchanges through the main oceanic gateways to the Arctic Ocean. *Oceanography*, *24*(3), 82–99. https://doi.org/10.5670/oceanog.2011.59

Björk, G., Gustafsson, B. G., & Stigebrandt, A. (2001). Upper layer circulation of the Nordic seas as inferred from the spatial distribution of heat and freshwater content and potential energy. *Polar Research*, *20*(2), 161–168. https://doi.org/10.1111/j.1751-8369.2001.tb00052.x

Blindheim, J. (1990). Arctic intermediate water in the Norwegian sea. *Deep Sea Research Part A. Oceanographic Research Papers*, *37*(9), 1475–1489. https://doi.org/10.1016/0198-0149(90)90138-L

Boehme, L., & Send, U. (2005). Objective analyses of hydrographic data for referencing profiling float salinities in highly variable environments. *Deep Sea Research Part II: Topical Studies in Oceanography*, *52*(3-4), 651–664. https://doi.org/10.1016/j.dsr2.2004.12.014

Bourke, R. H., Weigel, A. M., & Paquette, R. G. (1988). The westward turning branch of the West Spitsbergen Current. *Journal of Geophysical Research*, *93*(C11), 14,065–14,077.

Boyd, T. J., & D'Asaro, E. A. (1994). Cooling of the West Spitsbergen Current: Wintertime observations west of Svalbard. *Journal of Geophysical Research*, *99*(C11), 22,597–22,618.

de Boyer Montégut, C., Madec, G., Fischer, A. S., Lazar, A., & Iudicone, D. (2004). Mixed layer depth over the global ocean: An examination of profile data and a profile-based climatology. *Journal of Geophysical Research*, *109*, C12003. https://doi.org/10.1029/2004JC002378

Dickson, R. R., Meincke, J., Malmberg, S.-A., & Lee, A. J. (1988). The "great salinity anomaly" in the Northern North Atlantic 1968–1982. *Progress in Oceanography*, *20*(2), 103–151. https://doi.org/10.1016/0079-6611(88)90049-3

Eldevik, T., Nilsen, J. E. Ø., Iovino, D., Olsson, K., Sandø, A. B., & Drange, H. (2009). Observed sources and variability of Nordic Seas overflow. *Nature Geoscience*, *2*, 406–410. https://doi.org/10.1038/NGEO518

Fer, I., & Bosse, A. (2017). Seaglider missions in the Lofoten Basin of the Norwegian Sea, 2012–2015 (*Tech. rep.*): Geophysical Institute, University of Bergen (Norway). https://doi.org/10.21335/NMDC-UIB.2017-00018

Fer, I., Bosse, A., Ferron, B., & Bouruet-Aubertot, P. (2018). The dissipation of kinetic energy in the Lofoten Basin Eddy. *Journal of Physical Oceanography*, *48*, 1299–1316. https://doi.org/10.1175/JPO-D-17-0244.1

Flament, P. (2002). A state variable for characterizing water masses and their diffusive stability: Spiciness. *Progress in Oceanography*, *54*, 493–501.

Fossheim, M., Primicerio, R., Johannesen, E., Ingvaldsen, R. B., Aschan, M. M., & Dolgov, A. V. (2015). Recent warming leads to a rapid borealization of fish communities in the Arctic. *Nature Climate Change*, *5*(7), 673–677. https://doi.org/10.1038/nclimate2647

Furevik, T. (2001). Annual and interannual variability of Atlantic Water temperatures in the Norwegian and Barents Seas: 1980–1996. *Deep Sea Research Part I: Oceanographic Research Papers*, *48*(2), 383–404. https://doi.org/10.1016/S0967-0637(00)00050-9

Gary, S. F., Cunningham, S. A., Johnson, C., Houpert, L., Holliday, N. P., Behrens, E., et al. (2018). Seasonal cycles of oceanic transports in the eastern subpolar North Atlantic. *Journal of Geophysical Research: Oceans*, *123*, 1471–1484. https://doi.org/10.1002/2017JC013350

Hansen, B., & Østerhus, S. (2000). North Atlantic-Nordic Seas exchanges. *Progress in Oceanography*, *45*, 109–208.

Hattermann, T., Isachsen, P. E., Appen, W.-J., Albretsen, J., & Sundfjord, A. (2016). Eddy-driven recirculation of Atlantic Water in Fram Strait. *Geophysical Research Letters*, *43*, 3406–3414. https://doi.org/10.1002/2016GL068323

Holliday, N. P., Hughes, S. L., Bacon, S., Beszczynska-Möller, A., Hansen, B., Lavin, A., et al. (2018). Reversal of the 1960s to 1990s freshening trend in the northeast North Atlantic and Nordic Seas. *Geophysical Research Letters*, *35*, L03614. https://doi.org/10.1029/2007GL032675

Høydalsvik, F., Mauritzen, C., Orvik, K. A., LaCasce, J. H., Lee, C. M., & Gobat, J. (2013). Transport estimates of the western branch of the Norwegian Atlantic Current from glider surveys. *Deep-Sea Research Part I*, *79*, 86–95. http://www.sciencedirect.com/science/article/pii/S0967063713001027

Isachsen, P. E. (2015). Baroclinic instability and the mesoscale eddy field around the Lofoten Basin. *Journal of Geophysical Research: Oceans*, *120*, 2884–2903. https://doi.org/10.1002/2014JC010448

Isachsen, P. E., Koszalka, I., & LaCasce, J. H. (2012). Observed and modeled surface eddy heat fluxes in the eastern Nordic Seas. *Journal of Geophysical Research*, *117*, C08020. https://doi.org/10.1029/2012JC007935

Isachsen, P. E., Mauritzen, C., & Svendsen, H. (2007). Dense water formation in the nordic seas diagnosed from sea surface buoyancy fluxes. *Deep Sea Research Part I: Oceanographic Research Papers*, *54*(1), 22–41. https://doi.org/10.1016/j.dsr.2006.09.008

Ivanov, V., Alexeev, V., Koldunov, N. V., Repina, I. A., Sandoe, A. B., Smedsrud, L. H., & Smirnov, A. (2016). Arctic ocean heat impact on regional ice decay: A suggested positive feedback. *Journal of Physical Oceanography*, *46*, 1437–1456. https://doi.org/10.1175/JPO-D-15-0144.1

Ivanov, V., & Korablev, A. A. (1995a). Formation and regeneration of the pycnocline lens in the Norwegian Sea. *Russian Meteorology and Hydrology*, *9*(9), 62–69.

Ivanov, V., & Korablev, A. A. (1995b). Dynamics of an intrapycnocline lens in the Norwegian Sea. *Russian Meteorology and Hydrology*, *10*, 32–37.

Jackett, D. R., & McDougall, T. J. (1985). An oceanographic variable for the characterization of intrusions and water masses. *Deep Sea Research Part A, Oceanographic Research Papers*, *32*, 1195–1207.

Köhl, A. (2007). Generation and stability of a quasi-permanent vortex in the Lofoten Basin. *Journal of Physical Oceanography*, *37*(11), 2637–2651. https://doi.org/10.1175/2007JPO3694.1

Kolodziejczyk, N., Reverdin, G., & Lazar, A. (2015). Interannual variability of the mixed layer winter convection and spice injection in the eastern subtropical North Atlantic. *Journal of Physical Oceanography*, *45*(2), 504–525. https://doi.org/10.1175/JPO-D-14-0042.1

Koszalka, I., LaCasce, J. H., Andersson, M., Orvik, K. A., & Mauritzen, C. (2011). Surface circulation in the Nordic Seas from clustered drifters. *Deep-Sea Research*, *58*(4), 468–485. https://doi.org/10.1016/j.dsr.2011.01.007

Kwon, Y.-O., Alexander, M. A., Bond, N. A., Frankignoul, C., Nakamura, H., Qiu, B., & Thompson, L. A. (2010). Role of the Gulf Stream and Kuroshio-Oyashio systems in large-scale atmosphere-ocean interaction: A review. *Journal of Climate*, *23*(12), 3249–3281. https://doi.org/10.1175/2010JCLI3343.1

Latarius, K., & Quadfasel, D. (2016). Water mass transformation in the deep basins of the Nordic Seas: Analyses of heat and freshwater budgets. *Deep Sea Research Part I: Oceanographic Research Papers*, *114*, 23–42. https://doi.org/10.1016/j.dsr.2016.04.012

Laurian, A., Lazar, A., Reverdin, G., Rodgers, K., & Terray, P. (2006). Poleward propagation of spiciness anomalies in the North Atlantic Ocean. *Geophysical Research Letters*, *33*, L13603. https://doi.org/10.1029/2006GL026155

Lilly, J. M. (2017). jlab: A data analysis package for Matlab, v. 1.6.5. http://www.jmlilly.net/jmlsoft.html

Lilly, J. M., Rhines, P. B., Schott, F., Lavender, K., Lazier, J., Send, U., & D'Asaro, E. (2003). Observations of the labrador sea eddy field. *Progress in Oceanography*, *59*(1), 75–176. https://doi.org/10.1016/j.pocean.2003.08.013

Lind, S., Ingvaldsen, R. B., & Furevik, T. (2018). Arctic warming hotspot in the northern Barents Sea linked to declining sea-ice import. *Nature Climate Change*, *8*, 634–639. https://doi.org/10.1038/s41558-018-0205-y

Loeng, H. (1991). Features of the physical oceanographic conditions of the Barents Sea. *Polar Research*, *10*, 5–18.

Mamayev, O. I. (1962). T-s curves and the vertical stability of ocean waters. *[In Russian.] Doklady Akademii Nauk SSSR*, *146*, 227–255.

Manley, T. O. (1995). Branching of Atlantic Water within the Greenland-Spitsbergen passage: An estimate of recirculation. *Journal of Geophysical Research*, *100*(C10), 20,627–20,634.

Marshall, J., & Schott, F. (1999). Open-ocean convection: Observations, theory, and models. *Reviews of Geophysics*, *37*, 1–64.

McDougall, T. J. (1989). Stream functions for the lateral velocity vector in a compressible ocean. *Journal of Marine Research*, *47*(2), 267–284. https://doi.org/10.1357/002224089785076271

McDougall, T., & Barker, P. (2011). Getting started with TEOS-10 and the Gibbs Seawater (GSW) Oceanographic Toolbox. *SCOR/IAPSO WG127* (p. 28). ISBN 978-0-646-55621-5

McDougall, T., & Krzysik, O. (2015). Spiciness. *Journal of Marine Research*, *73*, 141–152. https://doi.org/10.1357/002224015816665589

Meyer, A., Fer, I., Sundfjord, A., & Peterson, A. K. (2017). Mixing rates and vertical heat fluxes north of Svalbard from Arctic winter to spring. *Journal of Geophysical Research: Oceans*, *122*, 4569–4586. https://doi.org/10.1002/2016JC012441

Mork, K. A., & Blindheim, J. (2000). Variations in the Atlantic inflow to the Nordic Seas, 1955–1996. *Deep Sea Research Part I: Oceanographic Research Papers*, *47*(6), 1035–1057. https://doi.org/10.1016/S0967-0637(99)00091-6

Mork, K. A., Skagseth, Ø., Ivshin, V., Ozhigin, V., Hughes, S. L., & Valdimarsson, H. (2014). Advective and atmospheric forced changes in heat and fresh water content in the Norwegian Sea, 1951–2010. *Geophysical Research Letters*, *41*, 6221–6228. https://doi.org/10.1002/2014GL061038

Munk, W. H. (1981). Internal waves and small-scale processes. In B. Warren & C. Wunsch (Eds.), *Evolution of Physical Oceanography* (pp. 264–290). Cambridge, MA: The MIT Press.

Nilsen, J. E. Ø. (2006). Falck, E. *Progress in Oceanography*, *70*(1), 58–90. https://doi.org/10.1016/j.pocean.2006.03.014

Nilsen, F., Gjevik, B., & Schauer, U. (2006). Cooling of the West Spitsbergen Current: Isopycnal diffusion by topographic vorticity waves. *Journal of Geophysical Research*, *111*, C08012. https://doi.org/10.1029/2005JC002991

Onarheim, I. H., Smedsrud, L. H., Ingvaldsen, R. B., & Nilsen, F. (2014). Loss of sea ice during winter north of Svalbard. *Tellus A: Dynamic Meteorology and Oceanography*, *66*(1), 23933. https://doi.org/10.3402/tellusa.v66.23933

Orvik, K. A., & Niiler, P. (2002). Major pathways of Atlantic water in the northern North Atlantic and Nordic Seas toward Arctic. *Geophysical Research Letters*, *29*(19), 1896. https://doi.org/10.1029/2002GL015002

Orvik, K. A., Skagseth, Ø., & Mork, M. (2001). Atlantic inflow to the Nordic Seas: Current structure and volume fluxes from moored current meters, VM-ADCP and SeaSoar-CTD observations, 1995–1999. https://doi.org/10.1016/S0967-0637(00)00038-8

Oziel, L., Neukermans, G., Ardyna, M., Lancelot, C., Tison, J.-L., Wassmann, P., et al. (2017). Role for atlantic inflows and sea ice loss on shifting phytoplankton blooms in the Barents Sea. *Journal of Geophysical Research: Oceans*, *122*, 5121–5139. https://doi.org/10.1002/2016JC012582

Peterson, A. K., Fer, I., McPhee, M. G., & Randelhoff, A. (2017). Turbulent heat and momentum fluxes in the upper ocean under Arctic sea ice. *Journal of Geophysical Research: Oceans*, *122*, 1439–1456. https://doi.org/10.1002/2016JC012283

Poulain, P.-M., Warn-Varnas, A., & Niiler, P. P. (1996). Near-surface circulation of the Nordic seas as measured by Lagrangian drifters. *Journal of Geophysical Research: Oceans*, *101*(C8), 18,237–18,258. https://doi.org/10.1029/96JC00506

Quadfasel, D., Rudels, B., & Kurz, K. (1988). Outflow of dense water from a Svalbard fjord into the Fram Strait. *Deep-Sea Research*, *35*, 1143–1150.

Raj, R. P., Johannessen, J. A., Eldevik, T., Nilsen, J. E., & Halo, I. (2016). Quantifying mesoscale eddies in the Lofoten Basin. *Journal of Geophysical Research: Oceans*, *121*, 4503–4521. https://doi.org/10.1002/2016JC011637

Rhines, P., Häkkinen, S., & Josey, S. A. (2008). Is oceanic heat transport significant in the climate system? In R. R. Dickson, et al. (Eds.), *Arctic-Subarctic Ocean Fluxes: Defining the Role of the Northern Seas in Climate* (pp. 87–109). Dordrecht, Netherlands: Springer. https://doi.org/10.1007/978-1-4020-6774-7-5

Richards, C. G., & Straneo, F. (2015). Observations of water mass transformation and eddies in the Lofoten Basin of the Nordic Seas. *Journal of Physical Oceanography*, *45*(6), 1735–1756. https://doi.org/10.1175/JPO-D-14-0238.1

Rossby, T., Ozhigin, V., Ivshin, V., & Bacon, S. (2009). An isopycnal view of the Nordic Seas hydrography with focus on properties of the Lofoten Basin. *Deep Sea Research Part I: Oceanographic Research Papers*, *56*(11), 1955–1971. https://doi.org/10.1016/j.dsr.2009.07.005

Rossby, T., Prater, M. D., & Søiland, H. (2009). Pathways of inflow and dispersion of warm waters in the Nordic seas. *Journal of Geophysical Research*, *114*, C04011. https://doi.org/10.1029/2008JC005073

Ruddick, B. (1983). A practical indicator of the stability of the water column to double-diffusive activity. *Deep Sea Research Part A, Oceanographic Research Papers*, *30*(10), 1105–1107. https://doi.org/10.1016/0198-0149(83)90063-8

Rudels, B., Björk, G., Muench, R. D., & Schauer, U. (1999). Double-diffusive layering in the Eurasian Basin of the Arctic Ocean. *Journal of Marine Systems*, *21*(1), 3–27. https://doi.org/10.1016/S0924-7963(99)00003-2

Schauer, U. (1995). The release of brine-enriched shelf water from Storfjord into the Norwegian Sea. *Journal of Geophysical Research*, *100*, 16,015–16,028.

Schauer, U., & Beszczynska-Möller, S. (2009). Problems with estimation and interpretation of oceanic heat transport—Conceptual remarks for the case of Fram Strait in the Arctic Ocean. *Ocean Science*, *5*(6), 487–494.

Schmitt, R. W., & Evans, D. L. (1978). An estimate of the vertical mixing due to salt fingers based on observations in the North Atlantic central water. *Journal of Geophysical Research*, *83*(C6), 2913–2919. https://doi.org/10.1029/JC083iC06p02913

Segtnan, O. H., Furevik, T., & Jenkins, A. D. (2011). Heat and freshwater budgets of the Nordic Seas computed from atmospheric reanalysis and ocean observations. *Journal of Geophysical Research*, *116*, C11003. https://doi.org/10.1029/2011JC006939

Skagseth, Ø., Furevik, T., Ingvaldsen, R., Loeng, H., Mork, K. A., Orvik, K. A., & Ozhigin, V. (2008). Volume and heat transport to the Arctic Ocean via the Norwegian and Barents Seas. In R. R. Dickson, J. Meincke, & P. Rhines (Eds.), *Arctic-subarctic ocean fluxes*. Dordrecht, Netherlands: Springer. https://doi.org/10.1007/978-1-4020-6774-7_3

Søiland, H., Chafik, L., & Rossby, T. (2016). On the long-term stability of the Lofoten Basin Eddy. *Journal of Geophysical Research: Oceans*, *121*, 4438–4449. https://doi.org/10.1002/2016JC011726

Søiland, H., & Rossby, T. (2013). On the structure of the Lofoten Basin Eddy. *Journal of Geophysical Research: Oceans*, *118*, 4201–4212. https://doi.org/10.1002/jgrc.20301

Stommel, H. (1962). On the cause of the temperature-salinity curve in the ocean. *Proceedings of the National Academy of Sciences*, *48*, 764–766.

Veronis, G. (1972). On properties of seawater defined by temperature, salinity and pressure. *Journal of Marine Research*, *30*, 227–255.

Vihma, T. (2014). Effects of Arctic sea ice decline on weather and climate: A review. *Surveys in Geophysics*, *35*(5), 1175–1214. https://doi.org/10.1007/s10712-014-9284-0

Voet, G., Quadfasel, D., Mork, K. A., & Søiland, H. (2010). The mid-depth circulation of the Nordic seas derived from profiling float observations. *Tellus A*, *62*(4), 516–529. https://doi.org/10.1111/j.1600-0870.2010.00444.x

Volkov, D. L., Belonenko, T. V., & Foux, V. R. (2013). Puzzling over the dynamics of the Lofoten Basin — A sub-Arctic hot spot of ocean variability. *Geophysical Research Letters*, *40*, 738–743. https://doi.org/10.1002/grl.50126

Volkov, D. L., Kubryakov, A. A., & Lumpkin, R. (2015). Formation and variability of the Lofoten basin vortex in a high-resolution ocean model. *Deep-Sea Research I*, *105*, 142–157. https://doi.org/10.1016/j.dsr.2015.09.001

Yeager, S. G., & Large, W. G. (2004). Late-winter generation of spiciness on subducted isopycnals. *Journal of Physical Oceanography*, *34*(7), 1528–1547. https://doi.org/10.1175/1520-0485(2004)034<1528:LGOSOS>2.0.CO;2

Yeager, S. G., & Large, W. G. (2007). Observational evidence of winter spice injection. *Journal of Physical Oceanography*, *37*(12), 2895–2919. https://doi.org/10.1175/2007JPO3629.1

Yu, L.-S., Bosse, A., Fer, I., Orvik, K. A., Bruvik, E. M., Hessevik, I., & Kvalsund, K. (2017). The Lofoten Basin Eddy: Three years of evolution as observed by Seagliders. *Journal of Geophysical Research: Oceans*, *122*, 6814–6834. https://doi.org/10.1002/2017JC012982